NAVAL POSTGRADUATE SCHOOL

MONTEREY, CALIFORNIA

THESIS

SIGNAL-TO-NOISE RATIO GAINS AND SYNCHRONIZATION REQUIREMENTS OF A DISTRIBUTED RADAR NETWORK

by

Sean M. Hurley

June 2006

Thesis Advisor:	Murali Tummala
Co-Advisor:	Phillip Pace

Approved for public release; distribution is unlimited

THIS PAGE INTENTIONALLY LEFT BLANK

REPORT DOCUMENTATION PAGE			*Form Approved OMB No. 0704-0188*
Public reporting burden for this collection of information is estimated to average 1 hour per response, including the time for reviewing instruction, searching existing data sources, gathering and maintaining the data needed, and completing and reviewing the collection of information. Send comments regarding this burden estimate or any other aspect of this collection of information, including suggestions for reducing this burden, to Washington headquarters Services, Directorate for Information Operations and Reports, 1215 Jefferson Davis Highway, Suite 1204, Arlington, VA 22202-4302, and to the Office of Management and Budget, Paperwork Reduction Project (0704-0188) Washington DC 20503.			
1. AGENCY USE ONLY *(Leave blank)*	**2. REPORT DATE** June 2006	**3. REPORT TYPE AND DATES COVERED** Master's Thesis	
4. TITLE AND SUBTITLE Signal-to-Noise Ratio Gains and Synchronization Requirements of a Distributed Radar Network		**5. FUNDING NUMBERS**	
6. AUTHOR(S) Sean M. Hurley			
7. PERFORMING ORGANIZATION NAME(S) AND ADDRESS(ES) Center for Joint Service Electronic Warfare Naval Postgraduate School Monterey, CA 93943-5000		**8. PERFORMING ORGANIZATION REPORT NUMBER**	
9. SPONSORING /MONITORING AGENCY NAME(S) AND ADDRESS(ES) Missile Defense Agency		**10. SPONSORING/MONITORING AGENCY REPORT NUMBER**	
11. SUPPLEMENTARY NOTES The views expressed in this thesis are those of the author and do not reflect the official policy or position of the Department of Defense or the U.S. Government.			
12a. DISTRIBUTION / AVAILABILITY STATEMENT Approved for public release; distribution is unlimited		**12b. DISTRIBUTION CODE**	
13. ABSTRACT (maximum 200 words)			

This thesis explores the potential benefits of two, three, and four-node distributed radar networks with the potential to provide a received SNR proportional to n^2 times that of a single-node system, where n is the number of nodes in the network. By plotting the Cassini curves for these distributed radar networks along with the Cassini curves of a monostatic radar system for the same level of received SNR, these benefits are graphically demonstrated. The SNR gains result in a much larger area of coverage for the distributed radar network compared to that of a power-equivalent monostatic radar. The impact of phase and pulse synchronization on a distributed radar network is also explored. By examining phase error and pulse error separately, and then examining their impact on the coverage areas of a two-node distributed radar network, the importance of synchronization to a distributed radar network is demonstrated.

14. SUBJECT TERMS Distributed Sensor Network, Distributed Radar, System of Systems, Sensor Network, Target Tracking, Signal-To-Noise Ratio, Synchronization, Cassini ovals, Cassini curves, Area of Coverage			**15. NUMBER OF PAGES** 79
			16. PRICE CODE
17. SECURITY CLASSIFICATION OF REPORT Unclassified	**18. SECURITY CLASSIFICATION OF THIS PAGE** Unclassified	**19. SECURITY CLASSIFICATION OF ABSTRACT** Unclassified	**20. LIMITATION OF ABSTRACT** UL

NSN 7540-01-280-5500

Standard Form 298 (Rev. 2-89)
Prescribed by ANSI Std. 239-18

THIS PAGE INTENTIONALLY LEFT BLANK

SIGNAL-TO-NOISE RATIO GAINS AND SYNCRONIZATION REQUIREMENTS OF A DISTRIBUTED RADAR NETWORK

Sean M. Hurley
Captain, United States Marine Corps
B.S., United States Naval Academy, 2000

Submitted in partial fulfillment of the
requirements for the degree of

MASTER OF SCIENCE IN ELECTRICAL ENGINEERING

from the

NAVAL POSTGRADUATE SCHOOL
June 2006

Author: Sean M. Hurley

Approved by: Professor Murali Tummala
                 Thesis Advisor

                 Professor Phillip E. Pace
                 Co-Advisor

                 Professor Jeffrey B. Knorr
                 Chairman, Department of Electrical and Computer Engineering

THIS PAGE INTENTIONALLY LEFT BLANK

ABSTRACT

This thesis explores the benefits of two, three, and four-node distributed radar networks with the potential to provide a received *SNR* proportional to n^2 times that of a single-node system, where n is the number of nodes in the network. By plotting the Cassini curves for these distributed radar networks along with the Cassini curves of a monostatic radar system for the same level of received *SNR*, these benefits are graphically demonstrated. The *SNR* gains result in a much larger area of coverage for the distributed radar network compared to that of a power-equivalent monostatic radar. The impact of phase and pulse synchronization on a distributed radar network is also explored. By examining the phase error and the pulse error separately, and then examining their impact on the coverage areas of a two-node distributed radar network, the importance of synchronization to a distributed radar network is demonstrated.

THIS PAGE INTENTIONALLY LEFT BLANK

TABLE OF CONTENTS

LIST OF FIGURES

LIST OF TABLES

THIS PAGE INTENTIONALLY LEFT BLANK

ACKNOWLEDGMENTS

I would first like to thank my wife, Crystal, and my daughter, Alyssa, who tolerated long days of class followed by longer nights of study. Without their patience and support, I would not have completed this work.

I would like to express my sincere gratitude to Professor Murali Tummala, my thesis advisor, for his patience and guidance in mentoring me through the process of completing this thesis. His advice kept me focused and on course, and taught me how to perform research and writing at the postgraduate level.

I would also like to thank my co-advisor, Professor Phillip Pace, who provided guidance and materials on the intricacies of radars; CDR Owens Walker, who helped me to focus my research and writing; and James Calusdian, who helped me put my ideas into Matlab.

THIS PAGE INTENTIONALLY LEFT BLANK

EXECUTIVE SUMMARY

The United States is currently in the process of designing a missile defense system to guard against the threat of missile attack. Traditional monostatic and bistatic radar systems are capable of detecting a missile targeting the U.S.; however, these systems must be physically large (in order to provide a large coverage area) and require great amounts of power to provide coverage over a sufficiently large enough area. A network of small, easily deployable sensors that are capable of operating under low power conditions over a dispersed area while returning a large signal provides an alternative to traditional radars. The use of a tactical sensor grid in a clandestine operation has the potential for use within the military. These physically small sensors are easily deployable, require low power, and can operate in remote areas.

A distributed sensor network is a network of sensors and processing devices interconnected by a communications system. Traditionally, such a network is characterized by a dense population of small, lightweight, low-power sensors that communicate wirelessly. Utilizing the communications system, the sensors work cooperatively to share information throughout the network. A distributed radar network, which is an example of an active distributed sensor network, is used in this thesis to model the behavior of a distributed sensor network. Given identical systems at all nodes, an isotropic scatterer as the target, noise-limited system performance, and synchronization across all transmitters and receivers, the received Signal-to-Noise Ratio (*SNR*) of a distributed radar network can be shown to be proportional to n^2 times that of a single-node system, where n is the number of nodes in the network.

The objective of this thesis is to demonstrate the potential benefits of a distributed radar network and to explore the synchronization requirements necessary to realize these benefits. Using coverage area as a metric, the distributed radar network performance is compared to that of a monostatic radar.

Cassini ovals have been used to illustrate the shape of the coverage area for a given received *SNR* of bistatic radar systems. In this thesis, the Cassini oval is extended to a more general Cassini curve, where the number of radar nodes considered, *n*, is three and four. After developing the means to plot the Cassini curves, a graphical comparison is made between a monostatic radar system and a distributed radar network. Using the monostatic radar system as a reference, the Cassini curves are plotted for distributed radar networks with $n = 2, 3,$ and 4, and the coverage area of the curves is compared.

To better understand the design constraints of a distributed radar network, this thesis explores the assumption of synchronization across all transmitters and receivers in the network. Of specific interest is the synchronization required of the transmitted pulses to ensure that they combine constructively upon reflection from the target. This study of synchronization encompasses phase and pulse. Phase synchronization refers to the phase difference between the sinusoids. As the phase difference between the sinusoids changes, the power of the combined sinusoid will change; therefore, the received *SNR* will change as well. Pulse synchronization refers to the degree to which the combining sinusoidal pulses overlap (and therefore combine) with each other. This determines the duration of the maximum *SNR* in the received pulse. This thesis will study phase and pulse synchronization by combining sinusoids with differing amounts of phase difference and pulse overlap. The affect of the loss of phase and pulse synchronization is demonstrated by plotting Cassini ovals for a synchronized system versus a system that has phase error, one that has pulse error, and a system that has both phase and pulse errors.

I. INTRODUCTION

The last decade has seen tremendous technological advancements in the field of networking. Internet and email service to home and office, cellular telephones with data service, Voice-Over-Internet-Protocol (VoIP) service, and sensor networking have led to a world that is interconnected on many levels. As the ability to provide networked services has increased, the means over which these services are provided has evolved. While still transmitted primarily over a wired medium, many of the services listed above are now available wirelessly. This development has added flexibility and mobility, and, in some cases, lower costs due to the reduced amount of infrastructure required in many wireless applications.

The growing emphasis on networked connectivity combined with the ability to build smaller, more powerful sensor devices has led to the concept of a "distributed sensor network". A distributed sensor network [1], "consists of a set of sensors, a set of processing elements, and a communications network interconnecting the various processing elements", in which the sensors number in the "tens to hundreds". Research into power efficient algorithms to govern the operation of distributed sensor networks, which would allow even smaller and more dispersed sensor nodes, promises to further expand the applications of sensor networks.

Sensors can be divided into two broad categories: passive and active. Typical examples of passive sensors are those that sense light, temperature, and pressure; these sensors simply receive a signal due to a physical phenomenon. In contrast, an active sensor transmits a signal and records the response in order to sense a targeted physical phenomenon. A radar is an example of an active sensor, which transmits electromagnetic pulses to gather information about a target. In contrast to a traditional radar system in which the radar nodes either transmit and receive their own pulses (monostatic) or one node transmits and another receives (bistatic), a distributed radar network makes use of both monostatic and bistatic modes. These networks share many of the characteristics described above; in this context, a radar node is comprised of a sensor, a processing

element, and a communications transceiver. Figure 1 illustrates a set of radar nodes acting as a distributed radar network.
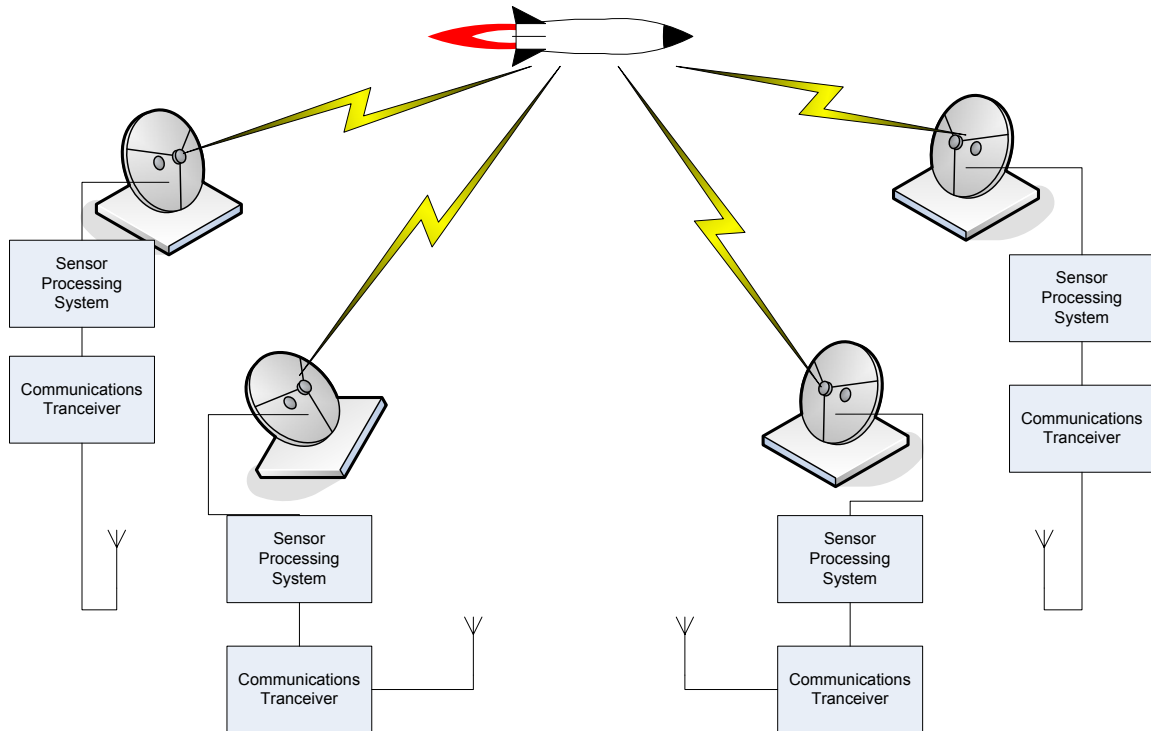
Figure 1.   A radar system acting as a distributed radar network. As sensors track a target, the nodes have the ability to process the data gathered and communicate with each other.

The attacks on September 11, 2001 have brought a renewed interest in the ability of the United States to defend itself against a missile attack. The effort to build a national missile defense system brings with it the requirement to be able to detect a missile launched at the United States which can be met by a distributed radar network that makes use of many small, independent, easily deployed, low power radars. By cooperatively sharing information across the network, a distributed sensor grid can be deployed over a sufficiently large area and still return a strong enough signal to detect and track the target. The advantages of a distributed radar network include more target perspectives resulting from the collective sharing of information gathered at each radar node [2] and a more

robust system that is not susceptible to a single point of failure. These advantages are particularly important in a missile defense system that has to detect and classify potential targets and non-targets.

Another military application for a distributed sensor network is the tactical employment of a passive sensor grid. In this mission, the sensors are laid in a manner to provide passive surveillance of an area of tactical value. In contrast to the missile defense scenario in which an active distributed radar network was appropriate, a passive distributed sensor network would provide the necessary surveillance while reducing the likelihood of detection by the enemy.

In both scenarios described, the distributed sensor network can also be deployed by airdropping the sensors from aircraft in order to form the sensor grid over land or sea. Air dropping the sensor nodes permits a rapid and flexible deployment means for the sensor grid, as described in [3].

The use of physically small, low powered sensors that still return a high Signal-to-Noise Ratio (*SNR*) has application in both missile defense (active distributed radar system) and tactical surveillance (passive distributed sensor system) missions. The small size of the sensors would make them easily deployable in both scenarios, and the low power would reduce the likelihood of the sensors being detected by an enemy. Additionally, the low power would allow the sensors to operate in a remote location [3], using a renewable power supply (e.g., sun, wind, etc.).

A.   RELATED WORK

Baker and Hume [2] lay out the theoretical and mathematical basis for the *SNR* gains of what they refer to as "netted radar system". This type of system shares information across the network in a cooperative and coherent manner to increase the overall *SNR* and provides multiple target aspect angles. Several assumptions about the system are made to allow the claim that a netted radar system returns *SNR* gains proportional to n^2 times that of a single-node system, where *n* is the number of sensor nodes in the network. These assumptions are identical systems at each node throughout

the network, synchronization across transmitters and receivers, an isotropic scatterer as the target, and noise limited system performance. Based on these assumptions, a netted radar range equation is developed. This thesis utilizes the netted radar work and studies the *SNR* gains, coverage areas, and the impact of synchronization on the *SNR* performance in a distributed radar network.

Willis [4] provides a comprehensive treatment of bistatic radar in which the transmitter and receiver are not collocated. The Cassini ovals are used to plot the shape of the coverage area. Additionally, the formulas necessary to compute the area within a given *SNR* oval are derived. This thesis extends the concept of Cassini curves for two nodes to three and four nodes.

B.   THE OBJECTIVE OF THIS THESIS

This thesis examines a distributed radar network to demonstrate the potential *SNR* advantage of distributed sensor networks. First, Cassini curves are developed by generalizing and extending Cassini ovals to three and four nodes. The formulas used to evaluate a bistatic radar system in [4] are extended to the case of three and four nodes, which enable the Cassini curves to be plotted. Second, the coverage area of a monostatic radar system is compared to that of a distributed radar network using these equations. Given a fixed *SNR,* the Cassini curves for a distributed radar network with two, three, and four nodes are presented and compared to those of a monostatic radar. This thesis also investigates the requirement for synchronization within a distributed radar network. By examining phase and pulse synchronization, the impact of synchronization on *SNR* gain is demonstrated.

C.   THE ORGANIZATION OF THIS THESIS

This thesis is organized as follows. Chapter II explores the concept of a distributed radar network, focusing on monostatic, bistatic, and systems with three and four nodes. The concept of a "Cassini curve" is introduced, and the equations required to plot these curves are extended from two to three and four sensor nodes. Chapter III uses the Cassini curves as a means to compare the distributed radar system to a monostatic

4

radar system. Chapter IV explores the synchronization requirement as it relates to the interaction of radar pulses at the target, and its effect on the resulting received *SNR*. Chapter V includes the contributions of this work and recommendations for follow-on research. The Appendix includes all Matlab code used to perform simulations and plots in the completion of this thesis.

THIS PAGE INTENTIONALLY LEFT BLANK

II.   DISTRIBUTED RADAR NETWORKS

Sensor networks are traditionally considered to be comprised of many small, randomly, and densely dispersed sensors that must perform the task of self-organizing into an operational network. The applications for sensor networks range from monitoring building temperature to battlefield surveillance. The military applications of sensor networks are of most interest to this thesis. A radar (sensor) is chosen as the means to examine the performance of a sensor network in this thesis.

A distributed radar system, in contrast to the monostatic or bistatic radar, incorporates all nodes into a large network across which information is shared. In addition to providing different target perspectives [2], a distributed radar network provides a received *SNR* proportional to n^2, where *n* is the number of sensor nodes in the network. This chapter introduces the radar systems that will be used in the evaluation of a distributed radar network and develops the means with which to compare these different systems.

A.   NETWORK OF RADARS

The operation of a distributed radar system depends on the number of nodes in the system. The number of nodes affects how the different nodes influence each other with respect to received *SNR*. A monostatic radar system, with one node, will be the reference system for use in evaluating the performance of a distributed radar network. This section develops the means to evaluate radar systems with different numbers of nodes.

1.   Monostatic Radar

A monostatic radar has one node consisting of a transmitter and a receiver as shown in Figure 2. The radar transmits a pulse toward the target, and receives a replica of this pulse after the target reflects it.

7
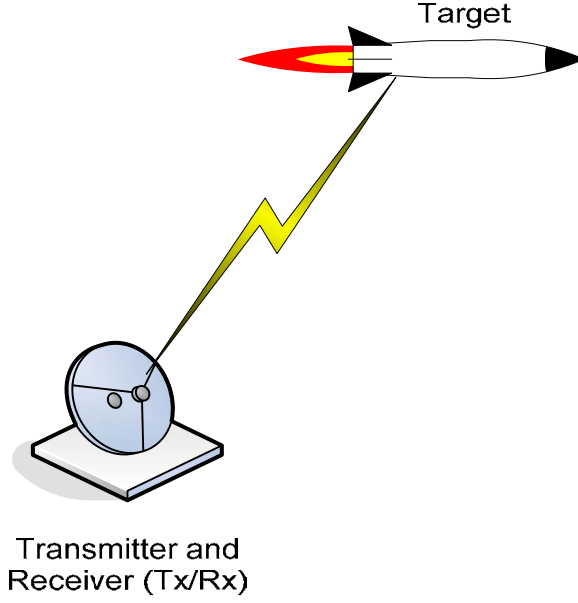
Figure 2.   A monostatic radar system.

The range equation for a monostatic radar is given by [5]:

$$R = \left[\frac{P_T G_T G_R \lambda^2 \sigma F^4}{(4\pi)^3 k T_s B_n (S/N)_{min} L} \right]^{1/4} \tag{2.1}$$

where R is the range from the radar to the target, P_T is transmitter power output, G_T is transmitting antenna gain, G_R is receiving antenna gain, λ is the carrier wavelength, σ is target cross section, F is the atmospheric attenuation factor, k is Boltzmann's constant, T_S is receiving system noise temperature, and B_n is the receiver's noise bandwidth, $(S/N)_{min}$ is the minimum *SNR* required for detection, and L accounts for various losses. Since there is one antenna, the coverage area given a constant set of input parameters resembles a circle around the radar. This causes the *SNR* to be constant at a given range:

$$\frac{S}{N} = \frac{P_T G_T G_R \lambda^2 \sigma F^4}{(4\pi)^3 k T_s B_n L R^4} \tag{2.2}$$

8

The lines of constant *SNR* around the node are called *SNR* contours; the geometric name for them is a Cassini curve. The circular shape of the *SNR* contours means that the area covered for a given *SNR* is the area within a circle [4]

$$A_M = \pi R^2 \tag{2.3}$$

where R is the distance from the node to a given Cassini curve.

2. Bistatic Radar

A bistatic radar system has a separate transmitter and a separate receiver. Distance d separates the transmitter and the receiver as shown in Figure 3. The transmitter emits a pulse toward the target, which reflects off the target and is detected by the receiver.
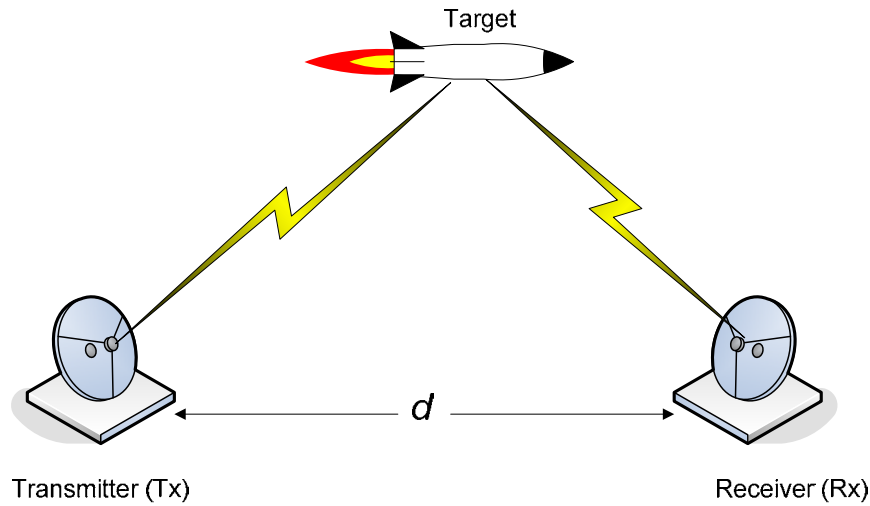
Figure 3.   A bistatic radar system in which the transmitter and the receiver are separated by a distance d.

For the bistatic radar, the maximum range equation is given by [4]

$$(R_T R_R)_{max} = \left[\frac{P_T G_T G_R \lambda^2 \sigma F_T^2 F_R^2}{(4\pi)^3 k T_S B_n (S/N)_{min} L} \right]^{1/2} = \kappa \tag{2.4}$$

where R_T is transmitter to target range, R_R is receiver to target range, F_T is the atmospheric attenuation factor from the transmitter to the target, F_R is the atmospheric attenuation factor from the target to the receiver, and κ is the bistatic maximum range product.

Willis [4] defines "ovals of Cassini" as "the locus of the vertex of a triangle when the product of the sides adjacent to the vertex is constant". The ovals of Cassini are a specific case of the Cassini curves in which $n = 2$. Each oval represents a constant SNR level; Figure 4 shows that R_T and R_R change as their intersection on a given SNR contour moves. The target position is considered to be this point of intersection. From Equation (2.4), the SNR of a bistatic radar is given by

$$\frac{S}{N} = \frac{P_T G_T G_R \lambda^2 \sigma F_T^2 F_R^2}{(4\pi)^3 kT_S B_n LR_T^2 R_R^2} \tag{2.5}$$
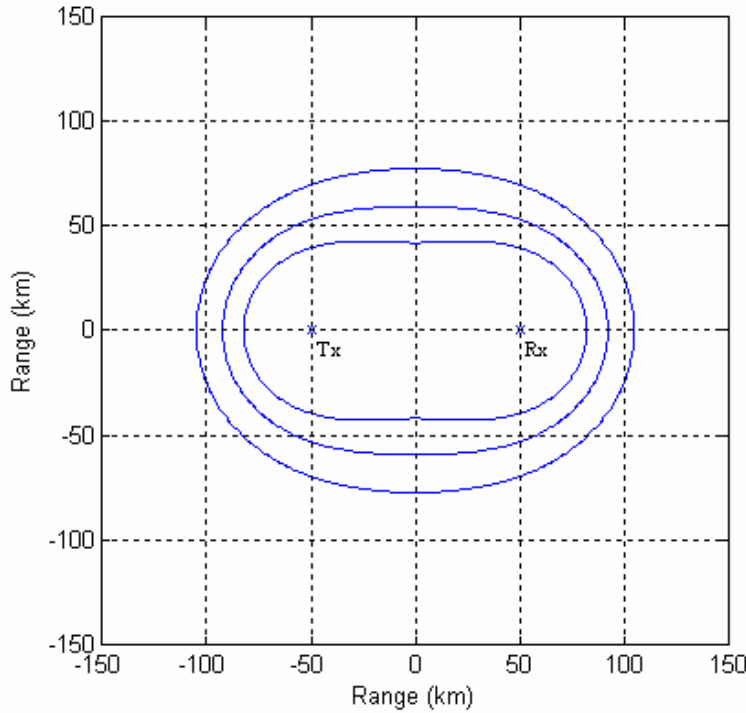
Figure 4.   Ovals of Cassini for a bistatic radar system. The separation distance d causes the SNR contours to appear oval in shape.

10

Willis also derives the area within the ovals of Cassini for a bistatic system, which can be used to compare different bistatic systems. This area is given as [4]

$$A_B = \pi\kappa\left[1 - \left(\frac{1}{2}\right)^2\left(\frac{d^4}{16\kappa^2}\right)^1\left(\frac{1}{1}\right) - \left(\frac{1\times3}{2\times4}\right)^2\left(\frac{d^4}{16\kappa^2}\right)\left(\frac{1}{3}\right) - \cdots\right]$$

$$\approx \pi\kappa\left[1 - \left(\frac{1}{64}\right)\left(\frac{d^4}{\kappa^2}\right) - \left(\frac{3}{16384}\right)\left(\frac{d^8}{\kappa^4}\right)\right].$$

(2.6)

3.   "Netted Radar"

The concept of netted radar is introduced in [2] in which several assumptions about the specific behavior of the system allow significant received *SNR* gains. The assumptions about the system are identical systems at each node throughout the network, synchronization across transmitters and receivers, an isotropic scatterer as the target, and noise limited system performance. Given these assumptions, the nature of such a distributed radar system allows the potential *SNR* gains to approach n^2, where *n* is the number of sensor nodes. Synchronization is the key requirement in order to realize this potential.

The general radar range equation [4] is modified to yield the range equation for the distributed radar [2]:

$$\frac{S}{N} = \sum_{i=1}^{n}\ \sum_{j=1}^{n}\frac{P_T G_T G_R \lambda^2 \sigma F_T^2 F_R^2}{(4\pi)^3 kT_S B_n R_{Ti}^2 R_{Rj}^2 L} = \sum_{i=1}^{n}\ \sum_{j=1}^{n}\left(\frac{S}{N}\right)_{ij}$$

(2.7)

where R_{Ti} is range from transmitter *i* to the target, R_{Rj} is range from receiver *j* to the target, and $\left(\frac{S}{N}\right)_{ij}$ is the *SNR* when node *i* is the transmitter and *j* is the receiver. The indices of summation are due to the collective nature of the system as every node transmits a pulse and all radars receive returns due to every transmitted pulse. Each of these actions contributes to the overall system *SNR*, resulting in the potential n^2 gains. Figure 5 illustrates the affect the indices of summation have on the total *SNR* for a distributed radar network with $n = 3$. The rows represent the summation over *i* and the columns represent the summation over *j*.

11

	$j = 1$	$j = 2$	$j = 3$
$i = 1$	Tx$_1$/Rx$_1$	Tx$_1$/Rx$_2$	Tx$_1$/Rx$_3$
$i = 2$	Tx$_2$/Rx$_1$	Tx$_2$/Rx$_2$	Tx$_2$/Rx$_3$
$i = 3$	Tx$_3$/Rx$_1$	Tx$_3$/Rx$_2$	Tx$_3$/Rx$_3$

Figure 5.   Matrix illustrating the indices of summation in Equation (2.7): each row represents the terms summed over i and each column represents the terms summed over j, resulting in n^2 *SNR* gains.

B.   CASSINI CURVES

In order to evaluate the performance of radar systems with different numbers of nodes, a means to plot these systems must be developed. This section expands the work done in [4] in order to develop a means to compare a monostatic radar system to a distributed radar system.

1.   General Expression for R

For any value of n, a Cassini curve is defined in [6] as "the curve for which the product of multiple polar radii is constant". This is a generalization of the definition of Cassini oval ($n = 2$) provided in [4], as described above. This definition is expressed as [6]:

$$\prod_{i=1}^{n} R_i = a \tag{2.8}$$

where n is the number of nodes, R_i is the radius from the ith node to a point on a Cassini curve (polar radii), and a is a constant. Following this result is the general equation for R, the distance from the origin to a point on a Cassini curve, given in polar form, which will plot a specific contour when given a value of n [6]:

12

$$R^n = 2\cos n\theta + \frac{a-1}{R^n}$$

where θ is the angle used in the polar plot ($0 \le \theta \le 2\pi$). Manipulating terms in the above equation yields the range from the origin to a point on a Cassini curve

$$R = r\sqrt[n]{\cos n\theta \pm \sqrt{a - \sin^2 n\theta}} \qquad (2.9)$$

where r is the radius from the origin to each node (and therefore dictates the size of the curves). The term of most interest in Equation (2.9) is a. The effect of a can be considered in three cases [6]:

- for $a < 1$, the curve consists of n pieces, each centered on a node.
- for $a > 1$, the curve is a Cassini oval, which becomes more circular as a grows.
- for $a = 1$, the curve is a sinusoidal spiral or lemniscate.

Of these, $a = 1$ is the most important case, and the word lemniscate (cusp) suggests that it is the border between the $a < 1$ and $a > 1$ cases. When $r = 1$, plots based on system input parameters can be obtained as shown in Figure 6.
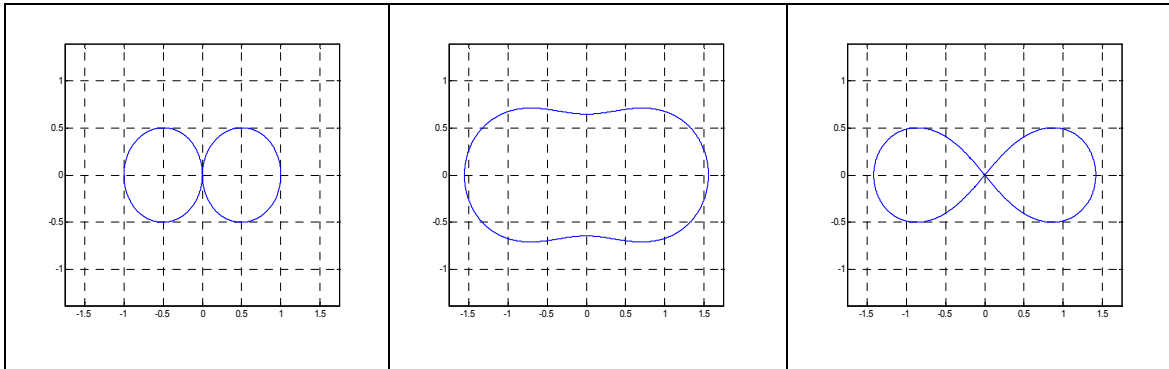
Figure 6.   Cassini curves plotted using Equation (2.9), illustrating the three cases for a (from left to right): $a < 1$, $a > 1$, and $a = 1$ $(r = 1, n = 2, 0 \le \theta \le 2\pi)$.

In order to make Equation (2.9) more specific, as well as provide a means to relate a and r to each curve, the geometry for each value of n to be considered

13

($n = 2, 3, 4$) is shown in Figure 7, along with the parameters associated with each shape [4], [7], and [8]. Here, d is the distance between nodes and r is the distance between a node and the origin O.

The geometry of the sensor network affects the variable r. As seen in Figure 7, r is different for each formation. In order to simplify the results for these shapes and provide a more general expression for R than Equation (2.9), the following values for r are established for $n = 2, 3, 4$ based on Figure 7 [4], [7], [8]:

$$r = \begin{cases} \dfrac{d}{2} & n = 2 \\ \dfrac{d}{\sqrt{3}} & n = 3 \\ \dfrac{d}{\sqrt{2}} & n = 4 \end{cases} \tag{2.10}$$

The derivation of R for a specific value of n, given the values for r listed above, begins with $n = 2$.

(a) line

14
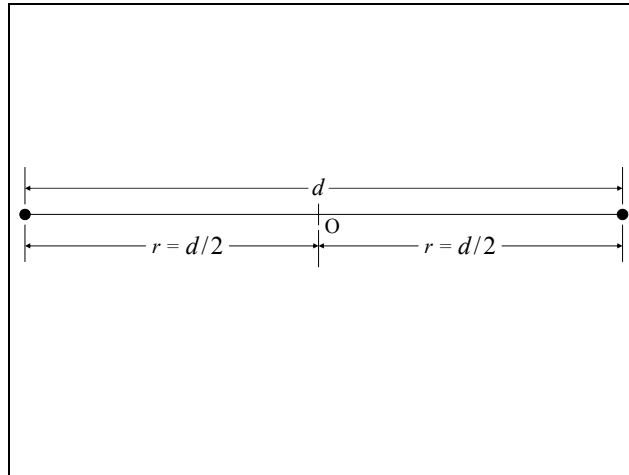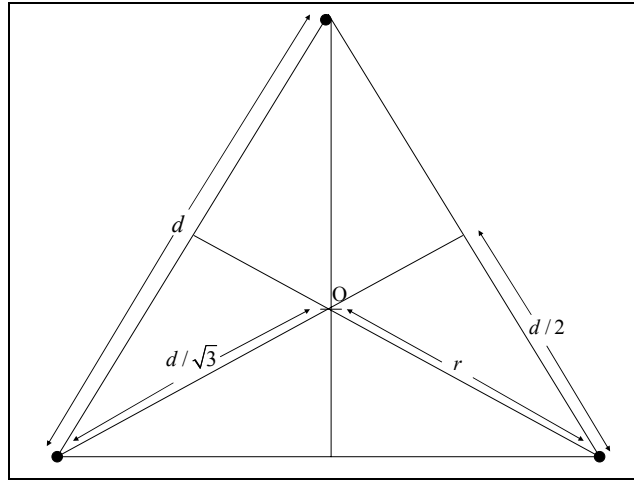
(b) equilateral triangle
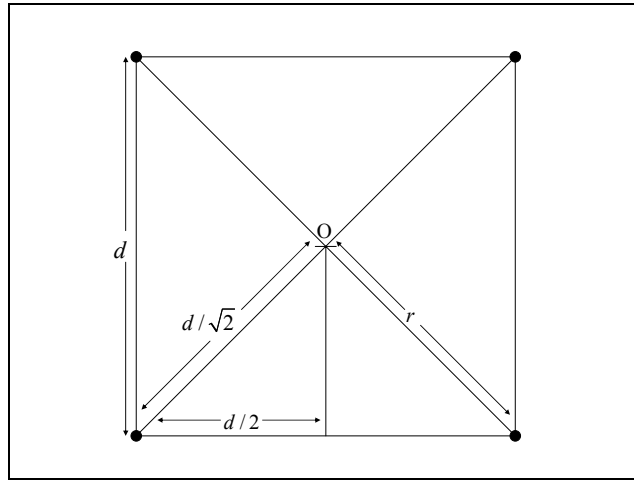
(c) square

Figure 7.   Geometry of the sensor nodes: (a) a line in which the nodes are placed at both ends of the line ($n = 2$); (b) an equilateral triangle in which the nodes are placed at each vertex ($n = 3$); (c) an array of four nodes forming a square grid ($n = 4$).

2. Two Nodes

Consider the geometry of a system with $n = 2$ from Figure 7(a). Figure 8 illustrates the various parameters for this case. By the Pythagorean Theorem, the ranges R_R and R_T can be expanded as [4]

$$R_R = \sqrt{\left(R^2 + \frac{d^2}{4}\right) - Rd \cos\theta} \qquad (2.11)$$

$$R_T = \sqrt{\left(R^2 + \frac{d^2}{4}\right) + Rd \cos\theta} \qquad (2.12)$$
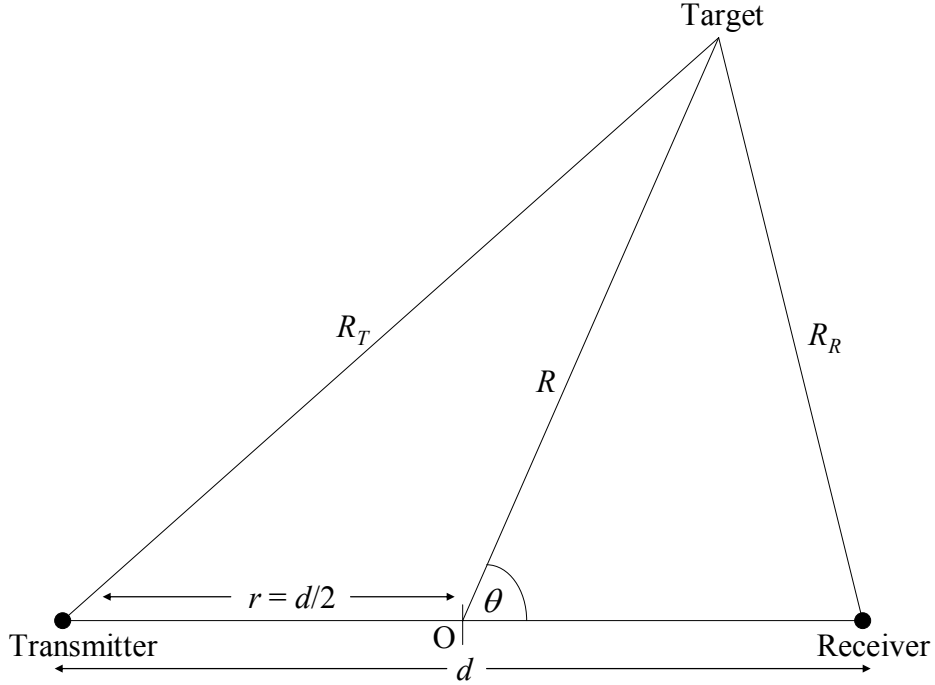
Figure 8.   A two-node distributed radar system, based on the geometry of a line from Figure 7(a). As the target moves, R, θ, R_T, and R_R change.

By taking the product of these two ranges, we have

$$R_T R_R = \kappa = \sqrt{R^4 + \frac{1}{2}R^2 d^2 + \frac{d^4}{16} - R^2 d^2 \cos^2\theta} \qquad (2.13)$$

By setting $\kappa = 0$, we can determine the distance from the origin to the target to be [4]

16

$$R^2 = \left(\frac{d}{2}\right)^2 \left[\cos 2\theta + \sqrt{\cos^2(2\theta) + \left(\frac{2\sqrt{\kappa}}{d}\right)^4 - 1} \right] \tag{2.14}$$

Comparing Equation (2.14) to Equation (2.9) for $n = 2$, we have the following expression for r and a:

$$r = \frac{d}{2} \tag{2.15}$$

$$a = \left(\frac{2\sqrt{\kappa}}{d}\right)^4 = \left(\frac{\sqrt{\kappa}}{r}\right)^4 \tag{2.16}$$

where $\kappa = R_T R_R$, and d is the separation of the sensor nodes. This result is expected given the geometry of Figure 7(a). For the case of $n = 2$, the three cases for a mentioned previously become [4]:

- for $d > 2\sqrt{\kappa}$, the curve consists of two ovals, each centered on a node,

- for $d < 2\sqrt{\kappa}$, the curve is one closed curve, and

- for $d = 2\sqrt{\kappa}$, the curve is a sinusoidal spiral or lemniscate.

It is important to note that the case of $a < 1$ has become $d > 2\sqrt{\kappa}$, and $a > 1$ has become $d < 2\sqrt{\kappa}$. These changes are a result of the geometry in Figure 7(a).

3.   Three Nodes

In the case of $n = 3$, the geometry of the system is somewhat more complex than that observed for the case of $n = 2$. After observing the derivation of R for the $n = 2$ case, including the value of $r = \frac{d}{2}$ and the fact that r scales the Cassini ovals to the desired distance from the origin, the same development is performed on R when $n = 3$. The geometry described in Figure 7(b) is used to set the scaling factor r, in the same manner that it was set for $n = 2$; therefore, for $n = 3$:

17

$$r = \frac{d}{\sqrt{3}} \tag{2.17}$$

$$a = \left(\frac{\sqrt{\kappa}}{r}\right)^4 = \left(\frac{\sqrt{3}\sqrt{\kappa}}{d}\right)^4 = \frac{9\kappa^2}{d^4} \tag{2.18}$$

and the three cases for Cassini curves become:

- for $d > \sqrt{3\kappa}$, the curve consists of three ovals, each centered on a node,

- for $d < \sqrt{3\kappa}$, the curve is one closed curve, and

- for $d = \sqrt{3\kappa}$, the curve is a sinusoidal spiral or lemniscate.

Again, the case of $a < 1$ has become $d > \sqrt{3\kappa}$, and $a > 1$ has become $d < \sqrt{3\kappa}$. These changes are a result of the geometry in Figure 7(b).

The coverage area in a radar system with $n = 3$ does not have the symmetry that is apparent in the case of a bistatic system. This increases the complexity of evaluating the area within the Cassini curves. Unlike the monostatic and bistatic cases, expressions to evaluate this area for systems with $n \geq 3$ have not been derived. Deriving such equations is beyond the scope of this thesis.

4.   Four Nodes

Assuming equally space nodes, the shape formed by four nodes is a square grid as seen in Figure 7(c). Following along the lines of the discussion above, we have

$$r = \frac{d}{\sqrt{2}} \tag{2.19}$$

$$a = \left(\frac{\sqrt{\kappa}}{r}\right)^4 = \frac{4\kappa^2}{d^4} \tag{2.20}$$

and the three cases for Cassini curves become:

18

- for $d > \sqrt{2\kappa}$, the curve consists of four ovals, each centered on a node,

- for $d < \sqrt{2\kappa}$, the curve is one closed curve, and

- for $d = \sqrt{2\kappa}$, the curve is a sinusoidal spiral or lemniscate.

The case of $a < 1$ has become $d > \sqrt{2\kappa}$, and $a > 1$ has become $d < \sqrt{2\kappa}$.

We remark that the development of the expression for R in the $n = 3$ and $n = 4$ cases above was performed from *observation* of the $n = 2$ case for which a complete derivation is available. A more rigorous derivation of R for these cases is beyond the scope of this work. The value of R (used to plot the Cassini curves) is dependant on r, which is based on the geometry of the sensor grid. Assuming equally spaced sensor nodes as in Figure 7, r is dependant on n.

This chapter focused on introducing the concept of distributed radar networks and developing the means with which to evaluate distributed radar networks versus a monostatic radar system. The parameter to be used in this evaluation is coverage area, which is plotted by Cassini ovals. Based on geometry and observation of the work in [4] for a bistatic radar, this chapter developed the expressions required to generate Cassini curves for systems with $n = 3$ and $n = 4$.

THIS PAGE INTENTIONALLY LEFT BLANK

III. COVERAGE AREA IN A DISTRIBUTED RADAR NETWORK

In this chapter, the coverage area of a distributed radar network will be examined. As a means of visually displaying the coverage area provided by a distributed radar network, the equations developed in Chapter II will be used to plot the Cassini curves. Monostatic and bistatic radar systems will be examined first, followed by distributed radar networks.

A. RADAR OPERATION

We begin with radar operations in which at a given time one node in the system transmits a pulse and the remaining nodes receive returns due to this pulse. First, the coverage area in a monostatic radar system will be examined by plotting Cassini curves for a given set of parameters. Next, the coverage area for two-node, three-node, and four-node radar systems will be plotted. The bistatic $(n = 2)$ case involves one node transmitting and one node receiving; the systems with $n = 3$ and $n = 4$ involve one node that transmits and several that receive the target returns. Since each system to be considered in this section (monostatic, bistatic, $n = 3$, and $n = 4$) has one transmitter, the total power for each system will be equal. The Cassini curves will be plotted for the same levels of *SNR* and compared to a monostatic radar for the same levels of *SNR*.

1. Monostatic Radar System

Willis [4] derives Equation (2.3) by taking the area of coverage of a bistatic radar system (discussed below) and setting inter-node spacing d to 0. The resulting shape of coverage is that of a circle. *SNR* decreases at an equal rate in all directions from the point of transmission, as seen in Figure 9, which shows the plots of the Cassini curves for a monostatic radar system. Each contour remains the same distance in all directions from the transmitter (labeled "Tx/Rx" and located at the origin); therefore, *SNR* remains the same for a given R. The *SNR* level at each curve from innermost to outermost is 12, 9, and 6 dB, respectively. The input parameters for the system used to generate the plot in Figure 9 are included in Table 1.

P_T (dBW)	G_T (dB)	G_R (dB)	f (GHz)	σ (dBsm)
10	8	8	10	10
F_T (dB)	F_R (dB)	T_S (K)	B_n (MHz)	L (dB)
-3.5	-3.5	300	60	1

Table 1.   Input parameters used to produce the plots in Figures 9, 10, 11, and 12.
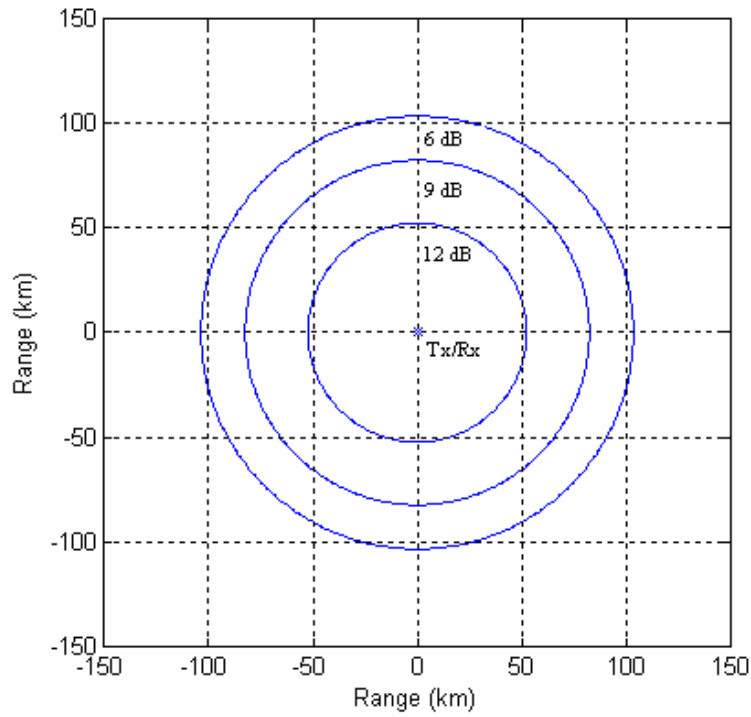
Figure 9.   Monostatic Cassini curves with the radar node located at the origin. The *SNR* of each curve is as marked.

2.   Bistatic Radar System

A bistatic radar operates by transmitting a pulse toward the target from the transmitter node. The receiver receives a copy of this pulse as reflected by the target. The resulting bistatic Cassini curves are due to the pulses transmitted by the transmitter and the target returns of those pulses received by the receiver.

22

The coverage area in a bistatic system is divided into two categories: detection constrained coverage and line-of-sight constrained coverage [4]. This thesis focuses on detection-constrained coverage, which refers to the coverage area that is defined by Equation (2.4). In other words, it is the area within a Cassini oval of a given received *SNR*. The input parameters to Equation (2.4) determine if it is possible to detect a target. Figure 10 shows the Cassini ovals for a bistatic radar system. The input parameters used to produce these curves are listed in Table 1. Given the input parameters of Table 1 and for an inter-node distance $d = 100$ km, the area within the 12 dB *SNR* curve seen in Figure 10 is calculated to be 1.2198×10^4 km^2. For the same *SNR*, the area for the monostatic radar in Figure 9 is 1.3421×10^4 km^2. Therefore, a monostatic radar covers slightly more area than a bistatic radar for the same level of received *SNR* [4]. This result is in accordance with Equations (2.3) and (2.6).

Both a monostatic and a bistatic radar have one transmitter; therefore, transmitted power (P_T) is equal for both systems. To better examine the results of increasing the number of nodes in the system, the total power throughout the system is kept equal when there is one transmitter in the system. Therefore, the same transmit power available for the monostatic system is available for the bistatic system.

In Figure 10, the *SNR* contours for the bistatic case are plotted in accordance with Equation (2.14) using the parameters of Table 1 and *d* set to 100 km. Figure 10 is plotted based on Figure 7(a). The transmitter is labeled "Tx" and the receiver is labeled "Rx". The coordinates of these radar nodes are (-50 km, 0) and (50 km, 0), respectively; each curve is for a constant value of *SNR*; from innermost to outermost curve the *SNR* levels are 12, 9, and 6 dB, respectively. The non-zero distance between the sensor nodes, *d*, results in an oval shape.
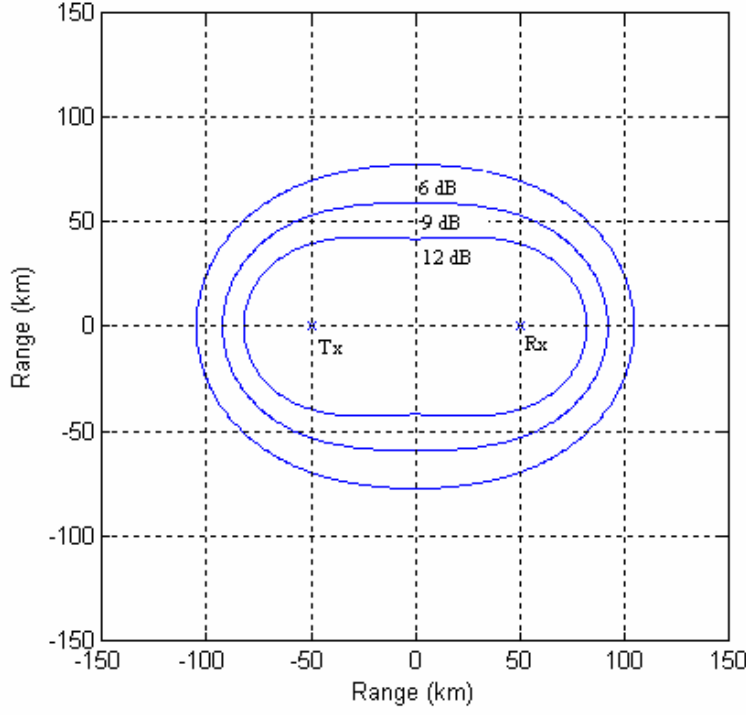
Figure 10. Bistatic Cassini ovals for a radar system with $n = 2$ in which the separation distance between the radar nodes results in the oval shape. The *SNR* values of the ovals are as marked.

3. Three Nodes

A radar system with $n = 3$ operates in a manner similar to a multistatic radar in which at a given time there is one transmitter and multiple receivers. In the case of a radar system with $n = 3$ considered here, one node transmits a pulse and a copy of this pulse is received by both of the other nodes after reflection from the target. The transmitting node does not receive a target return of its own transmitted pulses.

The input parameters for this case are listed in Table 1. The transmitted power (P_T) for the $n = 3$ case is equal to the transmitted power of the monostatic and bistatic cases because there is only one transmitter in the system.

Using Equations (2.9), (2.17) and (2.18), the *SNR* contours for the $n = 3$ case are plotted in Figure 11 using the parameters of Table 1 and the inter-node spacing d set to 100 km. Figure 11 is plotted based on Figure 7(b). The transmitting node is labeled "Tx" and the receiving nodes are labeled "Rx1" and "Rx2". The coordinates of these radar

24

nodes are (0, 57.735 km), (-50 km, -28.87 km), and (50 km, -28.87 km), respectively. The *SNR* level at each curve from innermost to outermost is 12, 9, and 6 dB, respectively. The lack of even symmetry is apparent from the odd number of nodes pictured. The fact that Rx1 and Rx2 do not transmit pulses results in the asymmetric shape of the Cassini curves between these nodes.
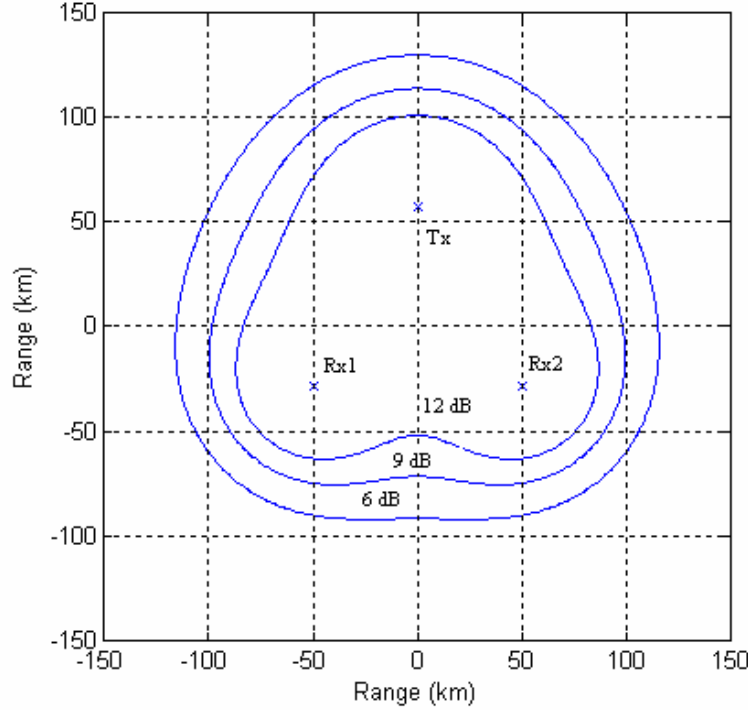
Figure 11.   Cassini curves for a radar system with $n = 3$. The *SNR* values of the ovals are as marked.

4.   Four Nodes

In the case of a radar system with $n = 4$ considered here, one node transmits a pulse and a copy of this pulse is received by the other three nodes after reflection from the target. The transmitting node does not receive target returns of its own transmitted pulses.

The input parameters for this case appear in Table 1. As in the previous cases, the transmitted power (P_T) for the $n = 4$ system is equal to the transmitted power of the monostatic system. Using Equations (2.9), (2.19) and (2.20), the Cassini curves for $n = 4$

are plotted in Figure 12 using the parameters of Table 1 and the inter-node distance d set to 100 km. Figure 12 is plotted based on Figure 7(c). The transmitting node is labeled "Tx" and the receiving nodes are labeled "Rx1", "Rx2", and "Rx3". The coordinates of these radar nodes are (-50 km, 50 km), (-50 km, -50 km), (50 km, -50 km), and (50 km, 50 km), respectively. The *SNR* level at each curve from innermost to outermost is 12, 9, and 6 dB, respectively. The even symmetry is apparent from the even number of nodes pictured. The fact that Rx1, Rx2, and Rx3 do not transmit pulses results in the asymmetric shape of the Cassini curves between these nodes.
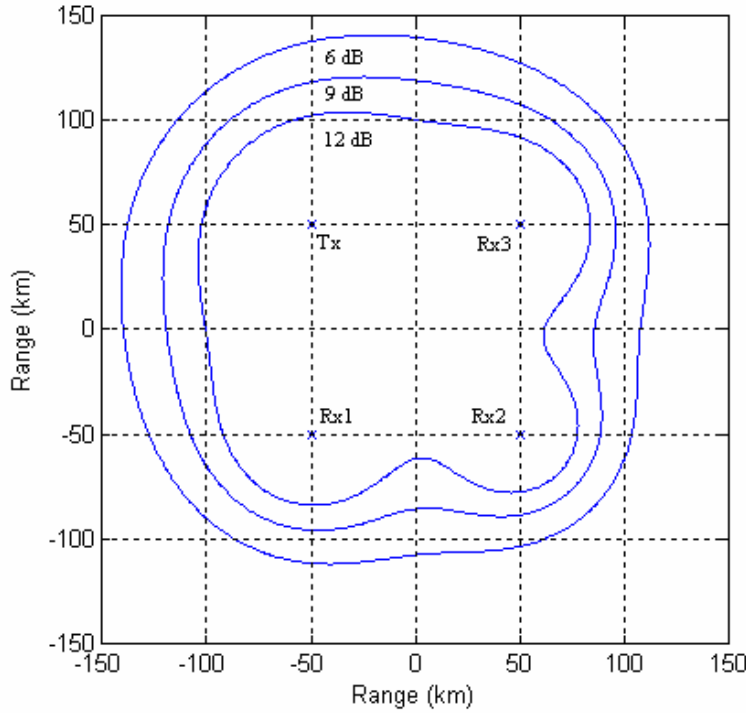
Figure 12.   Bistatic Cassini curves for a radar system with $n = 4$. The *SNR* values of the ovals are as marked.

B.   DISTRIBUTED RADAR NETWORKS

In this section, the coverage area of a two, three, and four-node distributed radar network will be evaluated and compared to the coverage area of a monostatic radar for the same received *SNR*. In a distributed radar network, every node transmits a pulse and all nodes (including the transmitter) receive copies of the transmitted pulse after it

reflects from the target. A distributed radar network is different from the two, three, and four-node radar systems described in Section A because every transmitter in a distributed radar network receives a target return of its own transmitted pulse (in addition to all other nodes receiving copies of the transmitted pulse).

1. Two-Node Distributed Radar Network

To compare the coverage area for a monostatic radar to the coverage area for the two-node distributed radar network, the two systems will be evaluated at the same levels of received *SNR*. The results will be presented graphically using Cassini curves.

a. *Transmission/Reception*

The *SNR* performance of a distributed radar network is described by Equation (2.7). The most important parts of that equation are the indices of summation. The subscripts i and j refer to which node in the system is transmitting and which node is receiving. Summing the *SNR* contributions from $i = 0$ to n and $j = 0$ to n gives the system its potential n^2 *SNR* gains. For the case of a two-node distributed radar, Equation (2.7) can be written as

$$\frac{S}{N} = \sum_{i=1}^{2} \sum_{j=1}^{2} \left(\frac{S}{N}\right)_{ij} = \left(\frac{S}{N}\right)_{11} + \left(\frac{S}{N}\right)_{12} + \left(\frac{S}{N}\right)_{21} + \left(\frac{S}{N}\right)_{22} \tag{3.1}$$

where $\left(\dfrac{S}{N}\right)_{11}$ and $\left(\dfrac{S}{N}\right)_{22}$ are monostatic *SNR*s of nodes 1 and 2, respectively, and $\left(\dfrac{S}{N}\right)_{12}$ and $\left(\dfrac{S}{N}\right)_{21}$ are bistatic *SNR*s of nodes 1 and 2, respectively, with the roles of transmitter and receiver assigned accordingly. When the target is placed at an equal distance from both nodes, we have the ranges

$$R_{T1} = R_{R1} = R_{T2} = R_{R2}$$

and consequently the *SNR*s

$$\left(\frac{S}{N}\right)_{11} = \left(\frac{S}{N}\right)_{22} = \left(\frac{S}{N}\right)_{12} = \left(\frac{S}{N}\right)_{21}$$

thereby yielding $\dfrac{S}{N} = 4\left(\dfrac{S}{N}\right)_{11}$, i.e., potential n^2 gains in received *SNR* compared to a single node radar case.

Another way of describing the gain to potential received *SNR* again results from the assumptions that the target is an isotropic scatterer located at an equal distance from all nodes, that each node illuminates the target with the same power, and that all nodes have identical system noise temperatures. Relative to the amplitude of a pulse from a single node, the amplitude of the pulses resulting from n nodes increases by n^2, resulting in an increase in signal power of n^4. Noise power and total transmitted power are increased by n compared to a single node. Therefore, the received *SNR* relative to a single node is proportional to n^2 [9].

Figure 13 illustrates the transmission and reception of pulses for $n = 2$. Transmitter 1 (Tx_1) emits a pulse (colored red), a copy of which is received by Receiver 1 (Rx_1) and Receiver 2 (Rx_2). Transmitter 2 (Tx_2) emits a pulse (colored blue), a copy of which is received by Receiver 2 (Rx_2) and Receiver 1 (Rx_1). The color-coding delineates which node is transmitting which pulse and the corresponding receivers. Overall, two pulses are transmitted ($n = 2$), and effectively four pulses are received (n^2 gains).
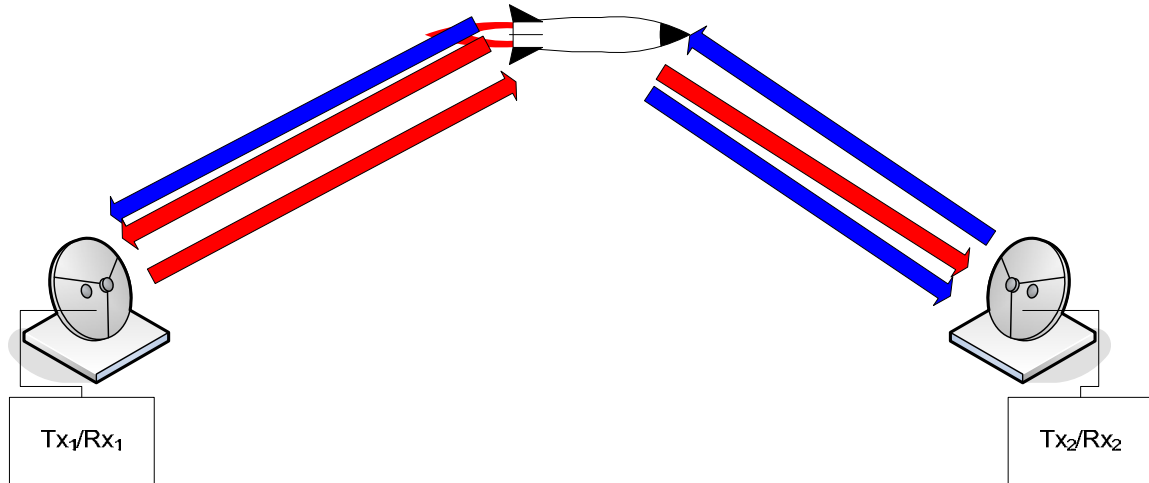
Figure 13.   Two-node distributed radar network illustrating two transmitted pulses and four received signals.

Figure 14 provides another perspective on Equation (2.7). Viewed as a matrix, the system has two transmitters and two receivers. Each row indicates the node referred to by i, and each column indicates the node referred to by j (i.e., Tx_i/Rx_j). For example, Tx_1/Rx_1 refers to node 1 transmitting its pulse ($i=1$) and receiving its own pulse ($j=1$); Tx_1/Rx_2 refers to node 1 transmitting its pulse ($i=1$) and receiving a pulse from node 2 ($j=2$). Again, two transmissions result in effectively four received pulses and n^2 gains are realized.
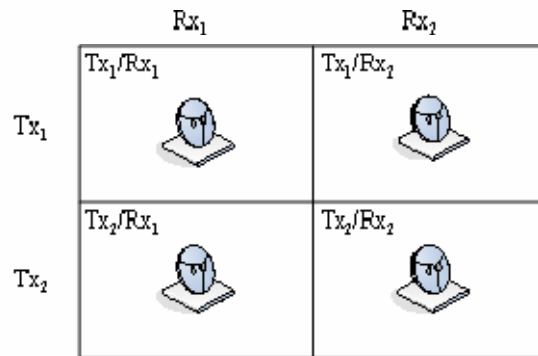
Figure 14.   Matrix illustrating how the subscripts i and j operate in Equation (2.7) for a two-node distributed radar network.

b.   *Coverage Area*

The shape of coverage area within a specific level of *SNR* is illustrated for the two-node distributed radar network and compared to that of a monostatic radar to demonstrate the potential gains of a distributed radar network. The input parameters for both systems are given in Table 1 except for the transmitted power (P_T) for the two-node distributed radar network, which is equal to half that for the monostatic case; this makes the two systems transmitted-power equivalent. To better examine the results of increasing the number of nodes in the distributed radar network, the total transmitted power of the system is kept equal regardless of the number of nodes involved.

The point of comparison between the two systems (monostatic and two-node distributed radar network) is the area within a Cassini curve for a given value of *SNR*. The comparison being made is based on a given *SNR* level, which is set equal for both systems in Figure 15. The monostatic node is plotted at the origin and the coordinates for the two-node distributed radar network nodes are the same as in Figure 10. The *SNR* level for the red curves is 6 dB, for the blue curves *SNR* is 9 dB, and for the green curves *SNR* is 12 dB. By observation, the two-node distributed radar network covers a noticeably larger area than the monostatic radar system. This is in contrast to the case considered in Chapter II, where the monostatic radar covered slightly more area than the bistatic radar. The fact that both nodes in the two node distributed radar network transmit a pulse and both nodes (including the transmitter) receive copies of the transmitted pulse after it reflects from the target causes the network to have a larger coverage area than the bistatic case (in which there is one transmitter and one receiver). This result is in accordance with Equation (3.1).
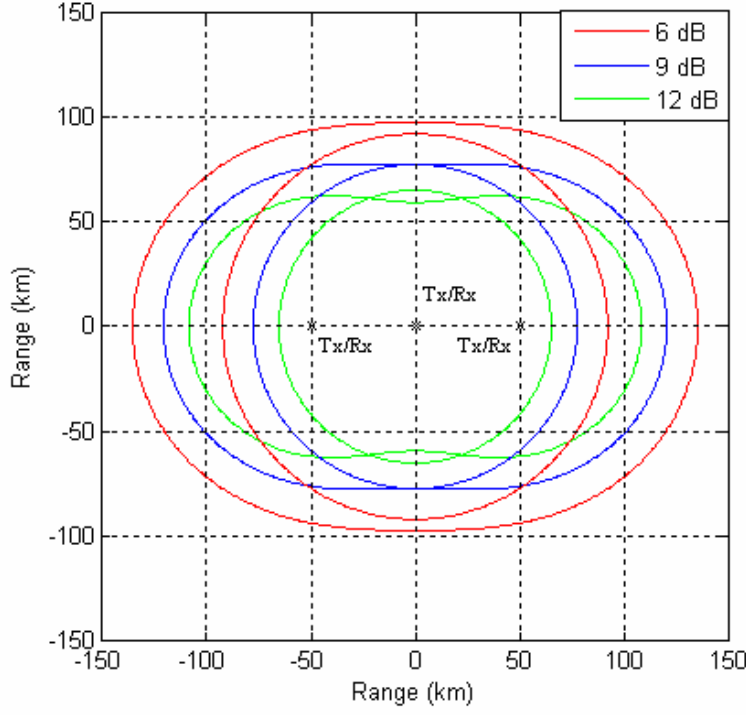
Figure 15. Comparison of coverage area between a two-node distributed radar network (ovals) versus a monostatic radar (circles). The red curves represent a received *SNR* of 6 dB, the blue curves represent a received *SNR* of 9 dB, and the green curves represent a received *SNR* of 12 dB.

2. Three-Node Distributed Radar Network

In this section, the shape of the coverage area within a three-node distributed radar network will be evaluated and compared to that of a monostatic radar for a given received *SNR*. To compare the coverage area at the same levels of received *SNR*, the results will be presented graphically using Cassini curves.

For the case of a three-node distributed radar network, Equation (2.7) offers the potential for a received *SNR* gains proportional to $n^2 = 9$ compared to that of a single node radar. This can be easily shown by following along the lines of the development of Equation (3.1). Figure 16 illustrates the transmission and reception of pulses. Each node transmits one pulse and each receives a pulse that is the combination of the three reflected pulses. This received pulse is color coded to show which transmitted pulses combine to form it.

31
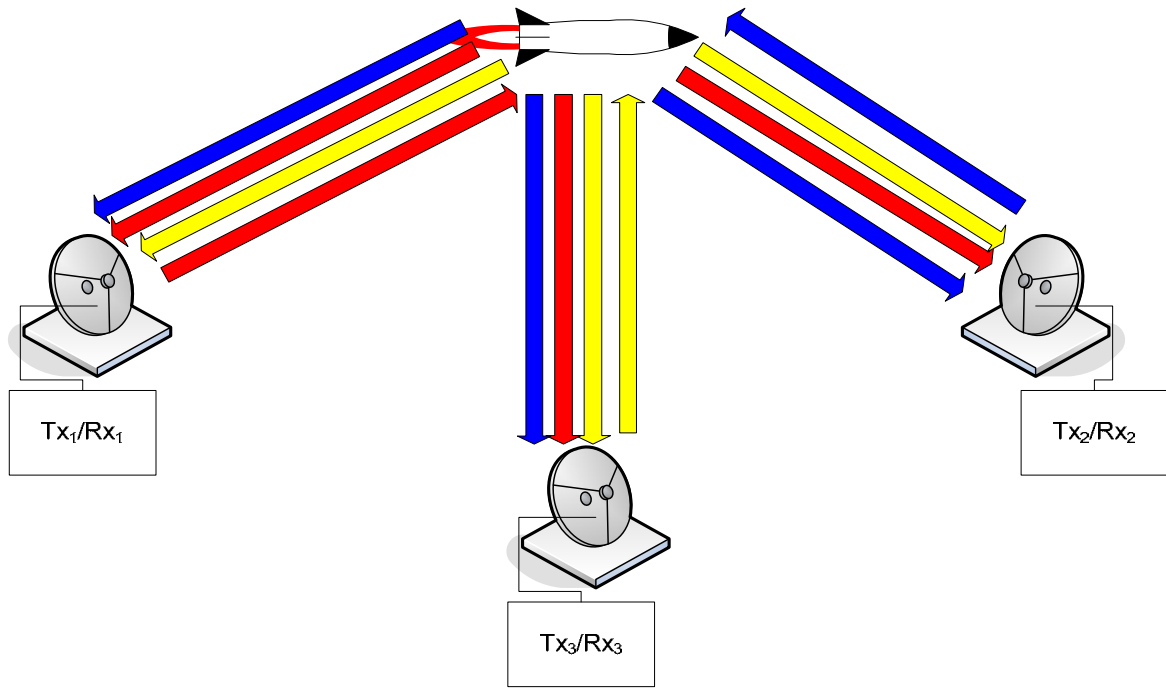
Figure 16. Three-node distributed radar network illustrating three transmitted pulses and nine received signals.

In Figure 17, the shape of coverage area within a specific level of *SNR* is illustrated for a three-node distributed radar network and compared to that of a monostatic system through the plots of Cassini curves for both systems. The input parameters for both systems are given in Table 1 except for the transmitted power of the three-node distributed radar network, which is one-third that of the monostatic case to provide a transmitted-power equivalent performance comparison of these two systems. The *SNR* levels in Figure 17 are represented by the same color-scheme as in Figure 15. The monostatic system is plotted at the origin and the three-node distributed radar network is plotted with the same coordinates as in Figure 11. By observation, the three-node distributed radar network covers a noticeably larger area than the monostatic radar system. Again, the difference between the three-node distributed radar network in Figure 17 and the radar system with $n = 3$ seen in Figure 11 is due to Equation (3.1).
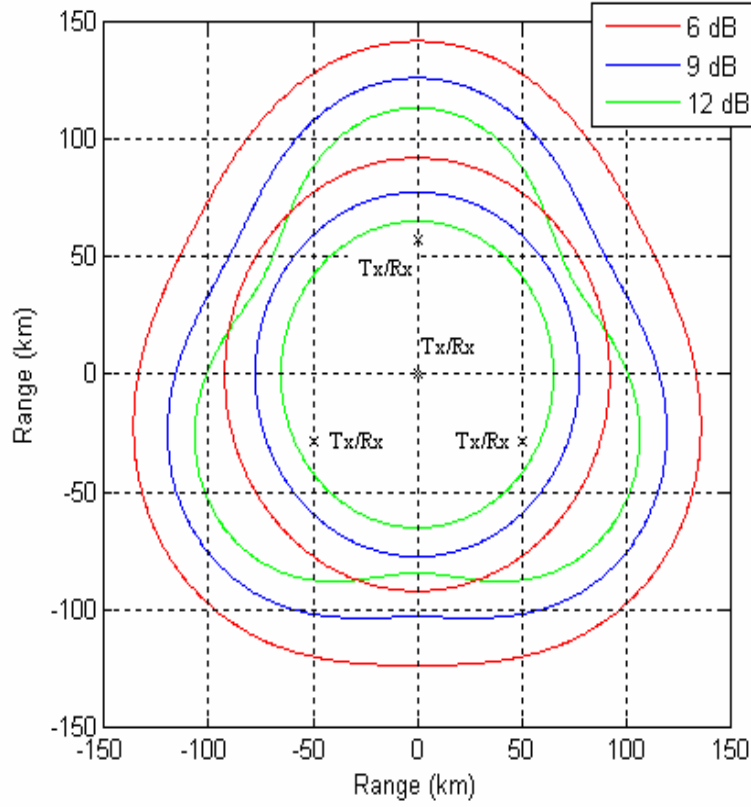
Figure 17.   Three-node distributed radar network Cassini curves (triangular curves) versus monostatic Cassini curves (circles). The *SNR* values of the curves are represented the same as in Figure 15.

3.   Four-Node Distributed Radar Network

In this section, the coverage area of a four-node distributed radar network will be evaluated and compared to the coverage area of a monostatic radar for the same received *SNR*. To compare the coverage area at the same levels of received *SNR*, the results will be presented graphically using Cassini curves.

For the case of a four-node distributed radar network, Equation (2.7) offers the potential for a received *SNR* gains proportional to $n^2 = 16$ compared to that of a single node radar. This can be easily shown by following along the lines of the development of Equation (3.1). Figure 18 illustrates the transmission and reception of pulses. Each node transmits one pulse and each receives a pulse that is the combination of the four reflected pulses. This received pulse is color coded to show which transmitted pulses combine to

form it. As in the previous cases, Equation (3.1) causes the four-node distributed radar network to cover a larger area than the radar system with $n = 4$ considered earlier in Figure 12.
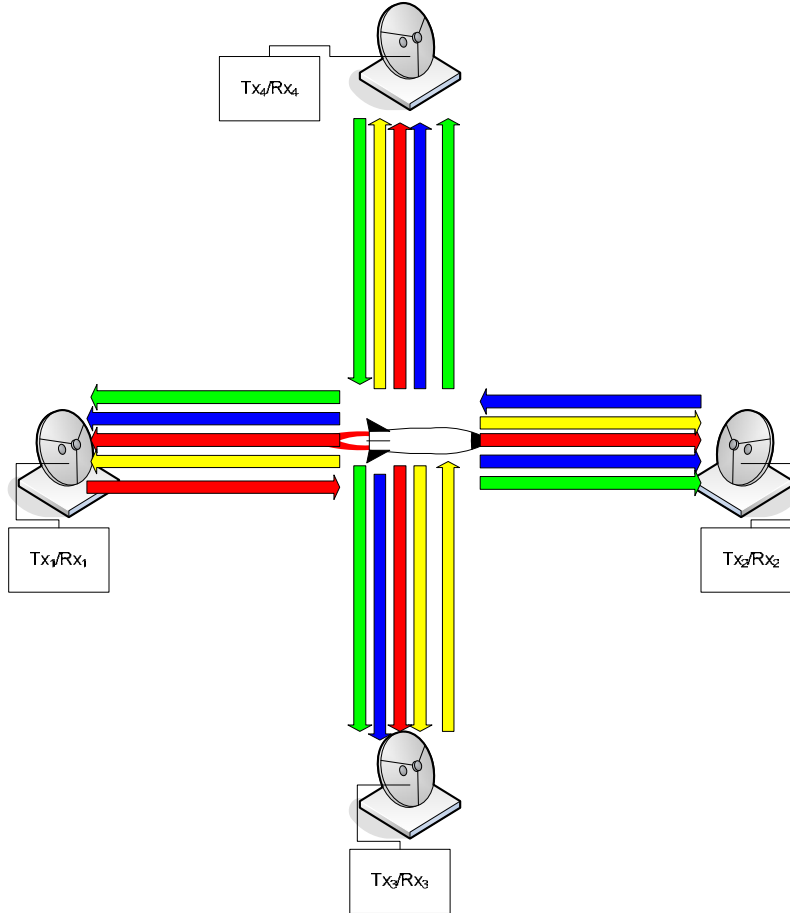
Figure 18.   Four-node distributed radar network illustrating four transmitted pulses and sixteen received signals.

The shape of coverage area within a specific level of *SNR* is illustrated in Figure 19 for a four-node distributed radar network and compared to that of a monostatic system through the plots of Cassini curves for both systems. The input parameters for both systems are given in Table 1 except for the transmitted power of the four-node distributed radar network, which is one-fourth that of the monostatic case; this allows us to make a transmitted-power equivalent comparison. As before, the monostatic system is plotted at the origin, the four-node distributed radar network is plotted at the same coordinates as

Figure 12, and the color-scheme is the same as in Figures 15 and 17. Again, by observation, the four-node distributed radar network covers a noticeably larger area than the monostatic radar system.
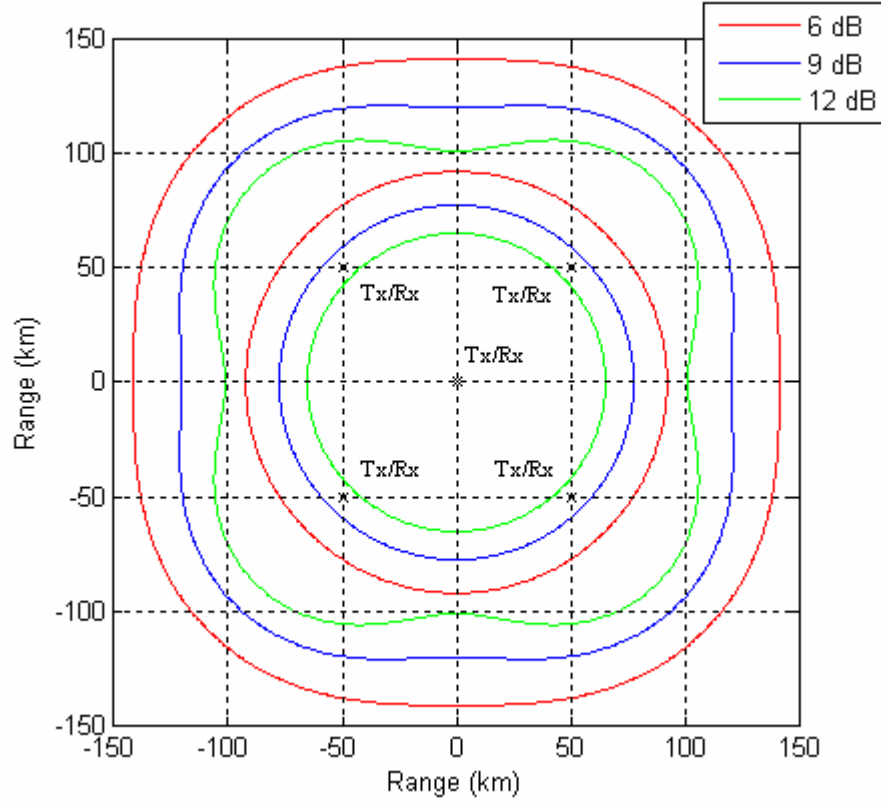
Figure 19. Four-node distributed radar network Cassini curves (square curves) versus monostatic Cassini curves (circles). The *SNR* values of the curves are represented the same as in Figures 15 and 17.

C. SUMMARY AND DISCUSSION

This chapter has graphically illustrated the shape of the coverage area of different types of radar systems by plotting the Cassini curves for each corresponding radar system. The first type of system evaluated was a monostatic system. In a monostatic system, the transmitter acts as its own receiver. In a bistatic system, there is a transmitter and a receiver. In the case of three-node and four-node systems, there is one transmitter and several receivers. The second type of system evaluated was the distributed radar

network in which every node receives its own pulse as well as those due to all other nodes. Cassini curves for $n = 2$, 3, and 4 are plotted along with those of a monostatic radar.

For a given level of received *SNR*, a distributed radar network results in a larger coverage area than a monostatic radar system, regardless of the number of nodes in the network ($n = 2, 3, 4$) as seen in Figures 15, 17, and 19. This is due to the fact that each node transmits a pulse and receives returns due to this transmitted pulse as well as the transmitted pulses from all other nodes in the distributed radar network. These results mean that by designing a radar network in such a way as to fulfill the requirements of Equation (2.7), the area of coverage of the network is significantly improved. The ability of the system to cooperatively share information potentially increases the received *SNR* proportional to n^2. If the network is not synchronized, the received *SNR* will not be increased proportional to n^2. The impact of synchronization on received *SNR* is investigated in Chapter IV.

IV. SYNCHRONIZING A DISTRIBUTED RADAR NETWORK

In this chapter, the requirements of synchronization in a distributed radar network will be examined. The topic of synchronization is essential to realizing *SNR* gains proportional to n^2 in a distributed radar network. We begin with a discussion of synchronization in a distributed radar network and then examine the phase and pulse synchronization. The causes and impact of synchronization loss on radar performance will be studied and both graphical and numerical results will be presented.

A. SYNCHRONIZATION AND A DISTRIBUTED RADAR NETWORK

Synchronization is a complex topic that encompasses time, frequency, and phase in a communication networking system. The scope and depth of discussion on synchronization in this work is limited to phase and pulse synchronization. The reader is reminded that all the other assumptions made with respect to Equation (2.7) still apply. Of specific relevance is the assumption that the target is an ideal isotropic reflector. Additionally, this chapter does not take into account electromagnetic propagation and field interactions.

1. Synchronization Issues

Two radar pulses are phase synchronized if they both reach their maximum amplitude at the same time. In order for the maximum *SNR* to be received, the separate pulses must add in such a manner as to maximize the amplitude of the combined reflected pulse as it *reflects off the target*, not as the individual pulses are transmitted. This point of combination at the target is the critical juncture at which the potential *SNR* gains are either maximized or lost.

Pulse synchronization refers to the amount of "overlap" of the pulse as it is reflected from the target (i.e., are the pulses completely overlapped, partially overlapped, or not overlapped?). If the pulses are completely synchronized (overlapped), the maximum power is reflected to the receiver. As this level of synchronization (overlap) is

reduced, the power of the pulse reflected to the receiver is also reduced. The reduction in signal power reduces the received *SNR*. Signal power is related to the received *SNR* as follows [10]

$$SNR = \frac{P_S}{\sigma_W^2} \qquad (4.1)$$

where P_S is signal power and σ_W^2 is the variance of additive white Gaussian noise. When the pulses are completely overlapped, the phase synchronization may or may not be achieved. As the amount of overlap decreases, the level of phase synchronization also changes.

In general, target tracking operations, such as those performed by a distributed radar network, require global knowledge of a reference time (i.e., a system clock) among the nodes that track the target [11]. The distributed radar system must share information among the nodes in order to coordinate transmission of pulses in such a way as to maximize the signal power of the pulses at the point of reflection from the target. This coordination allows the system to be synchronized in phase and pulse timing, thereby necessitating not only knowledge of time, but also of space (i.e., the nodes must know their location and the locations of their neighbors) [12]. A distributed radar system can reasonably be assumed to operate over a large geographic area with conditions (atmospheric, geographic, etc) that vary with time and/or space over this area, and can be left unattended for long periods of time [11]. The system must have a means of providing feedback to facilitate the coordination among all nodes that allows the system to adapt to changing conditions. This adjustment is made with the intent of changing pulse transmission parameters to maintain phase and pulse synchronization.

2. Causes of Synchronization Loss

Typically, synchronization is lost because the transmitted pulses do not arrive at the target at the intended time. This can be caused by an error in estimated target position or an error in pulse transmission time. The failure to transmit pulses so they reflect from

the target at the intended time is the main cause of synchronization loss as considered here. Later sections build on the discussion here to examine the performance impact of synchronization loss.

a.   *Error in Estimated Target Position*

There are several reasons why synchronization of pulses at the target might be lost. The first is an error in the estimation of the target position [13]. In this case, the pulses combine at the target, but not in a manner that allows a pulse combination resulting in maximum reflected power [4], thereby leading to a reduced signal power in the reflected pulse (i.e., destructive interference).

b.   *Pulse Transmission Timing Error*

A second reason for synchronization loss is error in the time of pulse transmission. The result of this error is that the transmitted pulses do not arrive at the target at the desired time (in order to synchronize upon reflection toward the receiver), causing a decrease in received *SNR*. A pulse transmission timing error can be caused by an error in the feedback algorithm or the software governing the operation of the system. A flaw in this software could lead to erroneous management of the transmission schedule, leading to the pulse transmission timing error [14]. If the system is unable to update the algorithm dictating the transmission schedule, it will not adjust properly to changing conditions within the area of operations. Finally, the clock tolerance of the system hardware may result in a level of precision in transmission timing that is not sufficient to synchronize the pulses.

B.   IMPACT OF SYNCHRONIZATION LOSS ON RECEIVED *SNR*

This section looks at synchronization loss due to phase error and pulse error and examines the effect these will have on the *SNR* of the pulse as it reflects from the target. The issues governing the combination of sinusoids and the time-limited nature of radar pulses are used to examine both phase and pulse synchronization. The simulation results are plotted for varying amounts of synchronization loss to illustrate the impact of this loss on the received *SNR*.

1.   Phase Error

Assume that n nodes simultaneously transmit one pulse aimed at a target as seen in Figure 1. These pulses arrive at the target at slightly different times, depending on the conditions in the medium between each node and the target as well as other sources of error discussed above. For this discussion, consider two sinusoidal pulses $y_1(t) = A\sin\omega_c t$ and $y_2(t) = A\sin(\omega_c t + \phi)$. As these pulses arrive, they will combine to yield [15]:

$$y_T(t) = y_1(t) + y_2(t) = (2A\cos\frac{1}{2}\phi)\sin(\omega_c t + \frac{1}{2}\phi) \qquad (4.2)$$

where A is the magnitude, ω_c is carrier frequency, and ϕ is the phase error between the two pulses. Due to this error ϕ, the magnitude of the reflected pulse is given by

$$\left|y_T(t)\right| = 2A\cos\frac{1}{2}\phi \qquad (4.3)$$

If $\phi = 0$ then $\left|y_T(t)\right| = 2A$; for non-zero values of $0 \le \phi \le 2\pi$, $\left|y_T(t)\right| < 2A$, which indicates a loss of magnitude. Consequently, the *SNR* of the reflected signal is [10]

$$SNR = \frac{\left(\dfrac{A'}{\sqrt{2}}\right)^2}{kT_s} = \frac{\left(\sqrt{2}A\cos\dfrac{1}{2}\phi\right)^2}{kT_S} \qquad (4.4)$$

where A' is the amplitude of the reflected sinusoidal pulse and A is the amplitude of the transmitted pulses; k is Boltzmann's constant and T_S is system noise temperature. Using this result with Equation (2.7), it is possible to realize n^2 *SNR* gains at even integer multiples of 2π phase error (i.e., perfect phase synchronization) or a complete loss of target return at odd integer multiples of π phase error (completely destructive interference). Between these extremes, there is a range of possible values for received *SNR*.

2.   Pulse Error

Pulse error is a measure of the amount of time overlap of the combining pulses at the point of combination. The duration of the pulses is finite and is assumed to be the same for all radar nodes in the network. Due to timing errors or target position estimation errors, the pulses may not overlap completely at the target. Additionally, some amount of phase error may also be present. Nevertheless, to maximize the signal power of the reflected pulse, we desire a complete overlap of pulses and zero phase error.

3.   Simulation Results

We now present the simulation results showing the effects phase error and pulse error on received *SNR*. Initially, phase error is considered separately from pulse error. Pulse error is then considered alone. Finally, the effects of both phase error and pulse error together on received *SNR* are considered.

a.   *Phase Error*

A plot of Equation (4.4) is shown in Figure 20, which illustrates the relationship between the normalized received *SNR* and the phase error (in radians) between the combining pulses. The received *SNR* decreases from a normalized maximum of 0 dB as phase error is increased. When phase error is zero, the interference between the pulses is constructive, resulting in the maximum amplitude. The interference between the pulses grows more destructive as phase error increases to a maximum plotted value of π radians, at which point the received *SNR* reaches its minimum value.
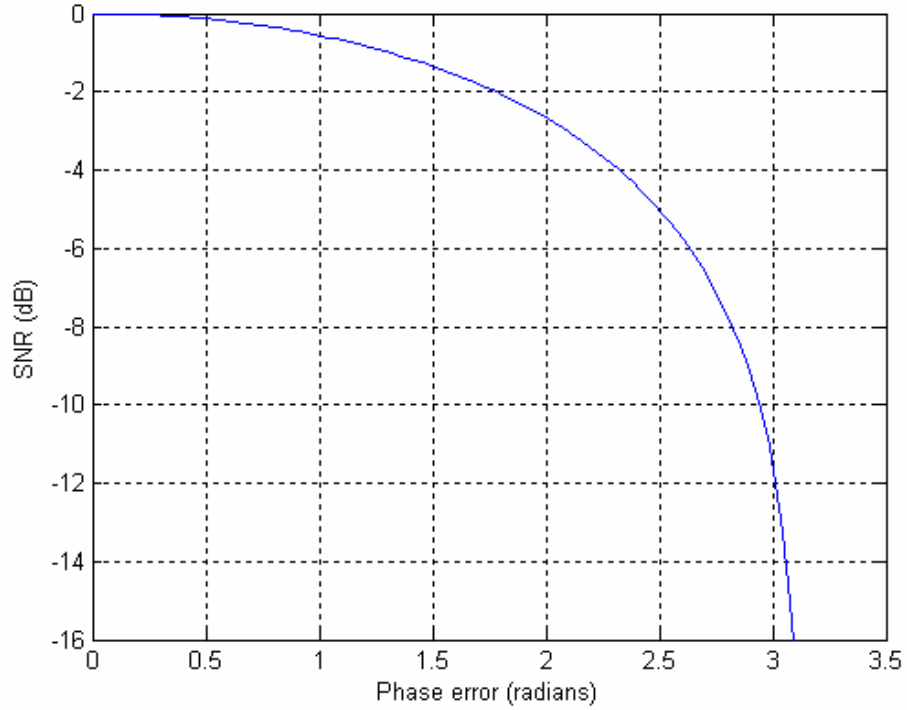
Figure 20. Received normalized *SNR* versus phase error (radians). As the phase error between the combining pulses increases to π radians, received *SNR* decreases.

Figure 21 shows the results of phase error on the Cassini curves of a two-node distributed radar network. The red curve is the Cassini curve for the two-node distributed radar network given perfect phase synchronization. The green curve is the Cassini curve for the same system with synchronization loss due to a 45° phase error. This corresponds to a normalized received *SNR* of 0 dB for the synchronized case (the red curve) versus –0.3 dB for the case with phase synchronization loss (the green curve).

Figure 21.   Cassini curves plotted for a two-node distributed radar network with synchronized pulses (red) versus curves plotted for a 45° phase error and zero pulse error (green).

b.   *Pulse Error*

Figure 22 shows the results of combining pulses with increasing amounts of pulse error. The pulse error is indicated in *time index* values. When the pulse error equals zero, the pulses are completely overlapped. Pulse error increases as the time index increases; therefore, *SNR* decreases as time index increases. When two pulses are completely overlapped, the received *SNR* is maximized, as seen at zero pulse error in Figure 22. When the pulse error increases, *SNR* decreases in a sinusoidal manner. As the amount of pulse error increases, the magnitude of the *SNR* reaches a terminal value, which is the *SNR* of an individual pulse. For simulation purposes, each pulse was modeled with a length of 500 time index values. Given a radar operating with a carrier frequency $f_c = 8$ GHz (i.e., in the X-band), each of these 500 time index values would represent 0.001 ns. It is emphasized that this pulse length is for simulation purposes only.
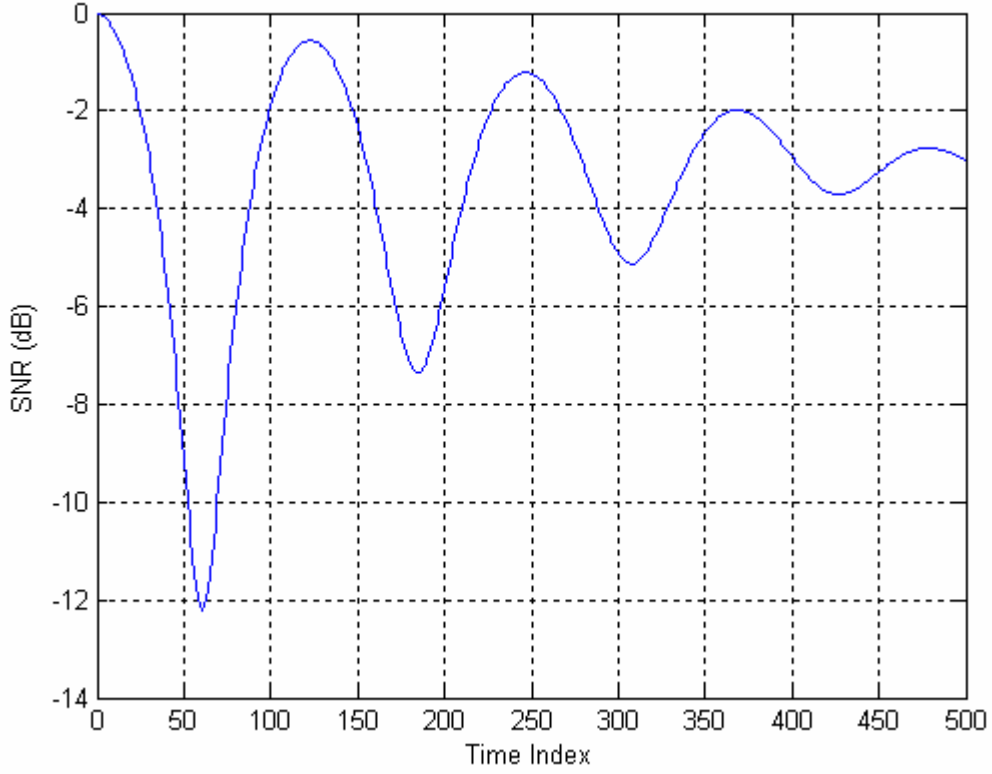
Figure 22.   Normalized received *SNR* versus pulse error (represented by Time Index). As the pulse error between the combining pulses increases, received *SNR* decreases in a sinusoidal manner.

Figure 23 illustrates the effect of pulse error on the amplitude of the resulting pulse in an *n*-node distributed radar network. As in Figure 22, the pulse error is indicated in time index values. The top row (in red) serves as a reference pulse; the second row (in blue) is a pulse that is shifted left along the Time Index axis (from the left column to the right column in each plot), and the third row (in green) is the combination of the two pulses above it in the same column. The case of partial overlap returns one pulse of length

$$l_p = 2t_1 - t_2 \tag{4.5}$$

where l_p is the length of the combined pulse, t_1 is the length of a transmitted pulse (pulse lengths are assumed to be the same), and t_2 is the length of the overlapping portion of the

44

two transmitted pulses as seen in Figure 23. For example, if there is no overlap, t_2 becomes zero and there are two pulses reflected with length $2t_1$. This figure displays only four cycles of each pulse to illustrate the concept of pulse combination with pulse error.
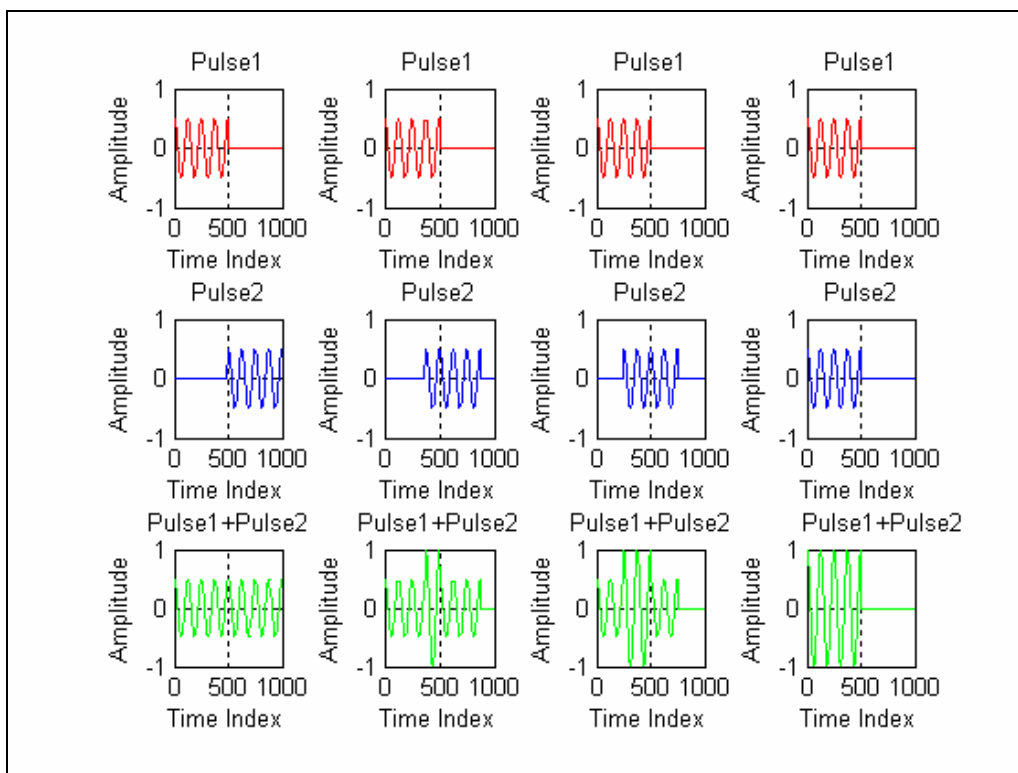
Figure 23. Pulse amplitude versus pulse error (represented by Time Index). The addition of pulses results in a combined pulse with an amplitude that is dependant on the amount of pulse error between the combining pulses.

Figure 24 shows the results due to pulse error on the Cassini curves of a two-node distributed radar network. The red curve is the Cassini curve for the two-node distributed radar network given perfect synchronization. The green curve is the Cassini curve for the same system with synchronization loss due to a pulse error of 375 time index values. This corresponds to a normalized received *SNR* of 0 dB for the synchronized case (the red curve) versus a normalized received *SNR* of -2.435 dB for the curve with a phase error of 0° and a pulse error of 375 time index values.
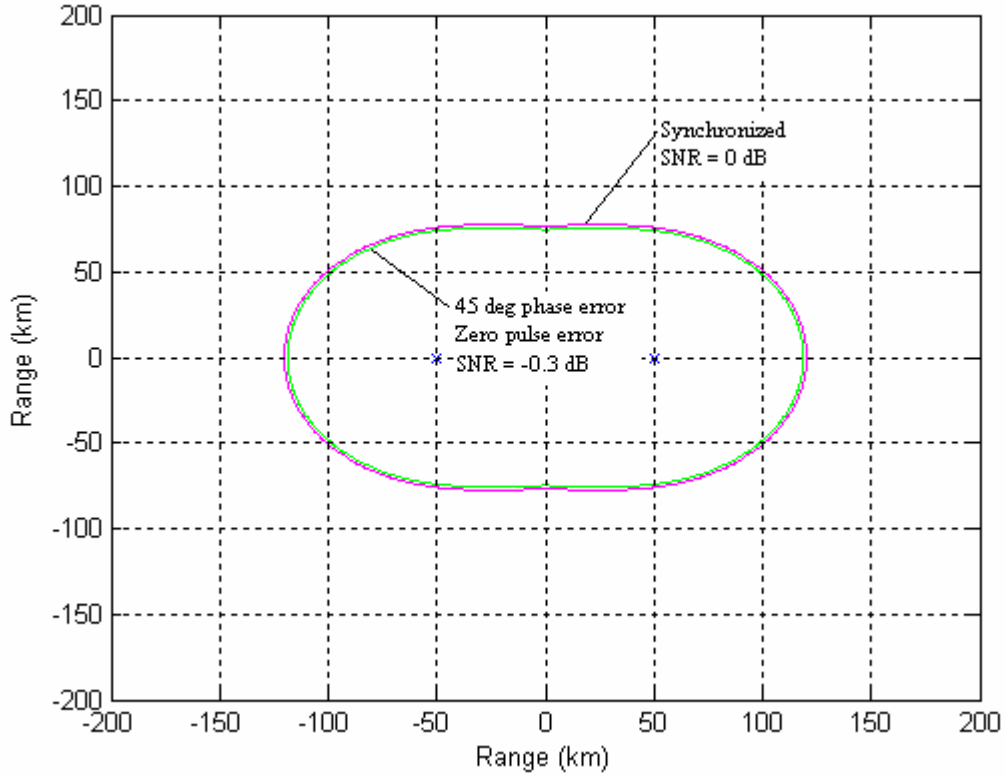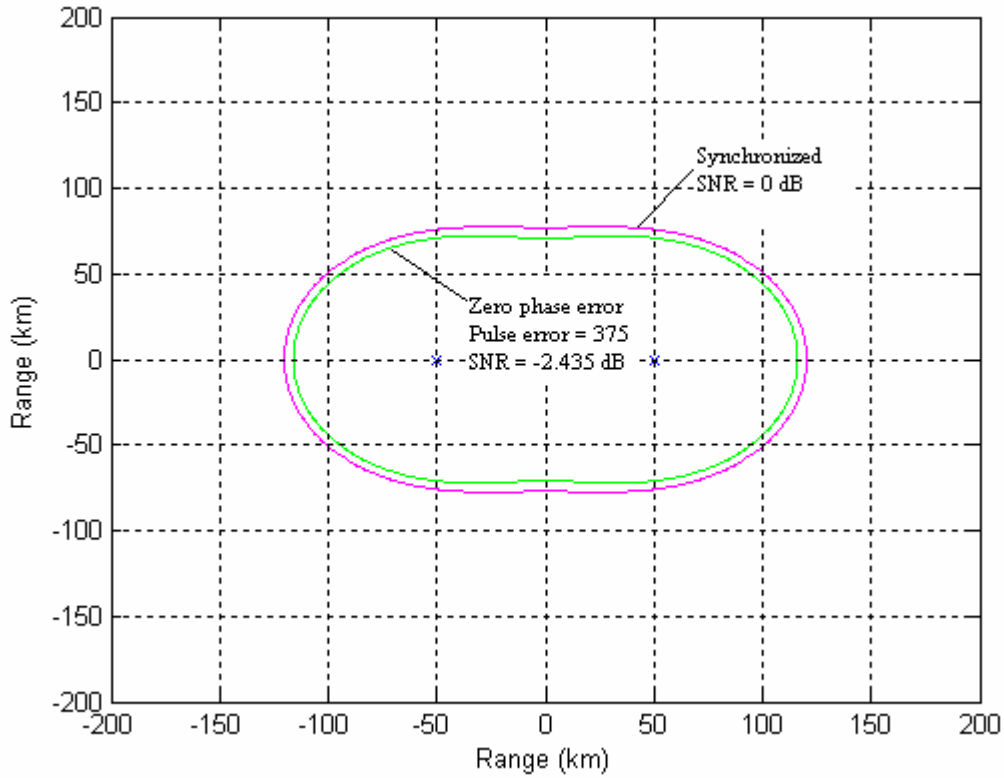
Figure 24.   Cassini curves plotted for a two-node distributed radar network with synchronized pulses (red) versus curves plotted for 0° phase error and a pulse error of 375 time index values between the two combining pulses (green).

c.   Simultaneous Phase and Pulse Error

We now consider the case of a two-node distributed radar network subjected to both phase error and pulse error. Figure 25 illustrates the pulse combination with both phase error and pulse error (indicated in time index values) included. The amount of pulse error is decreased from the left to the right columns, but the combining pulses have a phase error of 180°. Any portion of these pulses that overlap results in destructive interference. Phase error determines the amplitude of the combined portion of the pulse, the length of which is determined by the pulse error. In order to maximize the power of the reflected pulse, both phase error and pulse error must be minimized. Again, this figure displays only 4 cycles of each pulse to illustrate the concept of pulse combination with phase and pulse error.
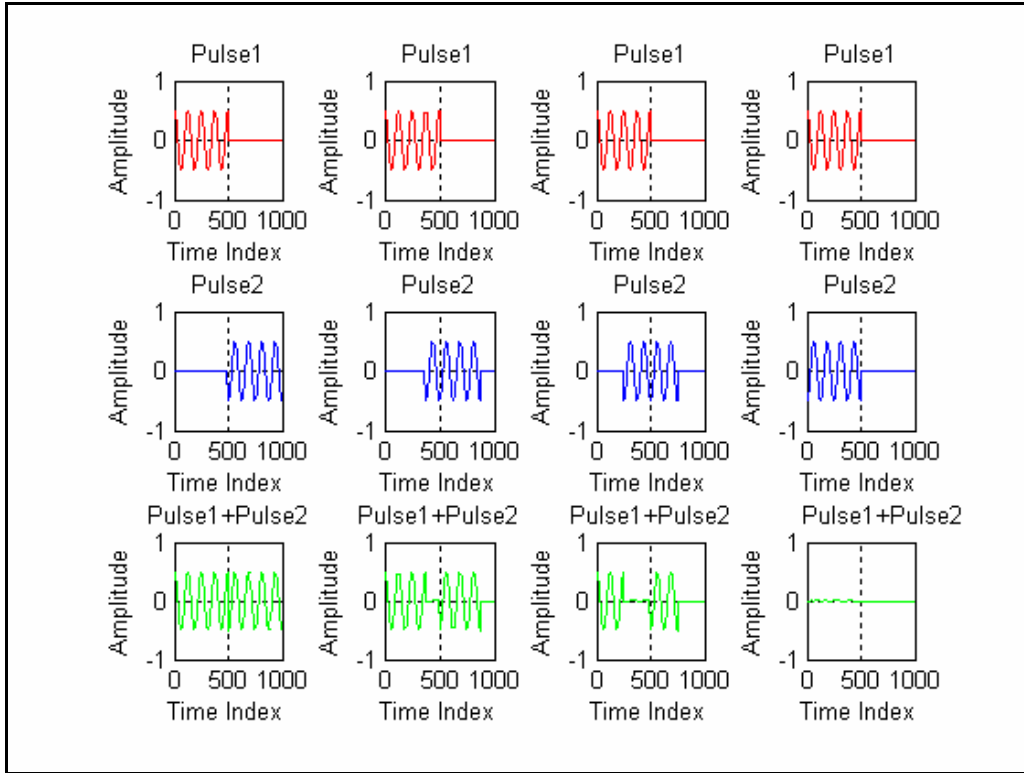
Figure 25.   The effect of 180° phase error on the combination of pulses with different amounts of pulse error (represented by Time Index). Any portion of the pulses that overlap combine destructively.

Table 2 summarizes the *SNR* values associated with Figures 20 and 22 as both pulse error and phase error are increased. The table shows that given two input pulses with zero phase error and zero pulse error, the resulting normalized received *SNR* is 0 dB. *SNR* decreases as overlap is decreased, approaching in a sinusoidal manner a value (in the case of this simulation) of approximately -3.04 dB. Since these values of *SNR* will be proportional to n^2, according to Equation (2.7), the larger value of *SNR* is clearly desirable in order to take advantage of the potential n^2 gains to received *SNR*.

		Pulse error			
P		0	250	375	500
h	0°	0	-1.217	-2.435	-3.04
a	45°	-0.3	-1.556	-3.407	-3.04
s	90°	-1.55	-2.741	-4.37	-3.04
e	180°	-16	-5.684	-3.368	-3.04

Table 2.   Normalized received *SNR* (dB) for given values of phase error and pulse error (represented by time index values).

Figure 26 illustrates the effect of both phase error and pulse error on received *SNR*. It shows that when there is zero pulse error, phase error causes the *SNR* to decrease (viewed along the axis labeled "Phase error (radians)"), which is also shown in Figure 20. As pulse error increases, *SNR* decreases in a sinusoidal manner, as also shown in Figure 22. The curve in Figure 26 is maximum at the origin (resulting from perfect synchronization) and slopes down as phase error is increased to a maximum plotted value of π radians (with pulse error constant at 0).
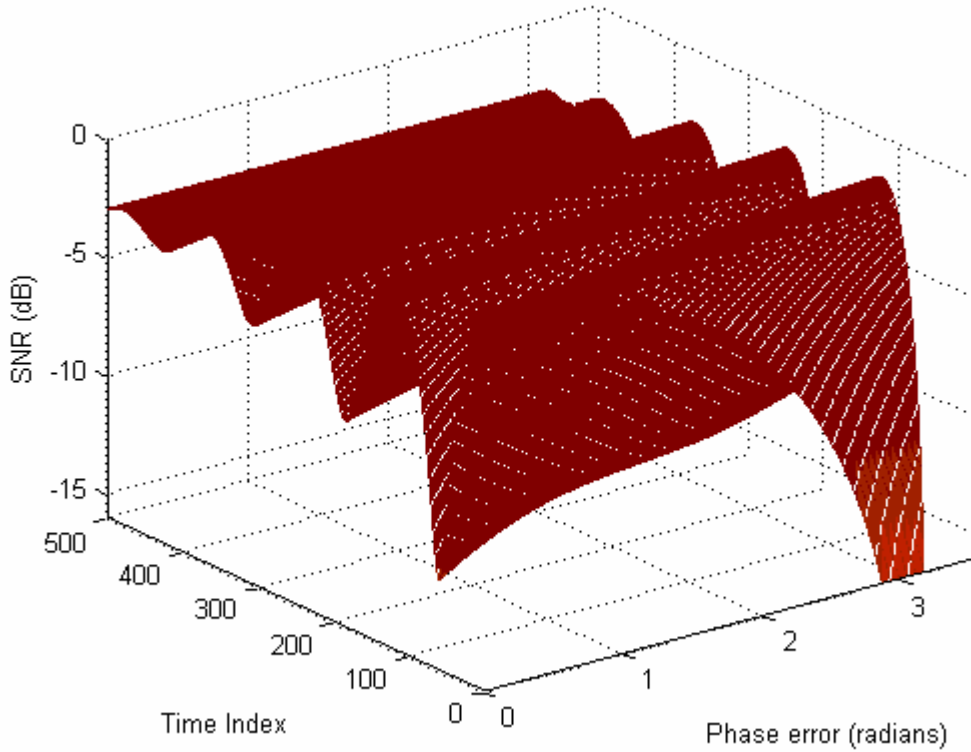
Figure 26.   Normalized received *SNR* versus phase error and pulse error. The effects of both phase and pulse error are plotted simultaneously.

Figure 27 plots the Cassini curve for perfect synchronization versus that for a phase error of 45° and pulse error of 375 time index values. This figure illustrates the effects of simultaneous occurrence of phase error and pulse error on the Cassini curves of a two-node distributed radar network. The coverage area for the curve with phase and pulse error is noticeably less than that for the case of perfect synchronization.
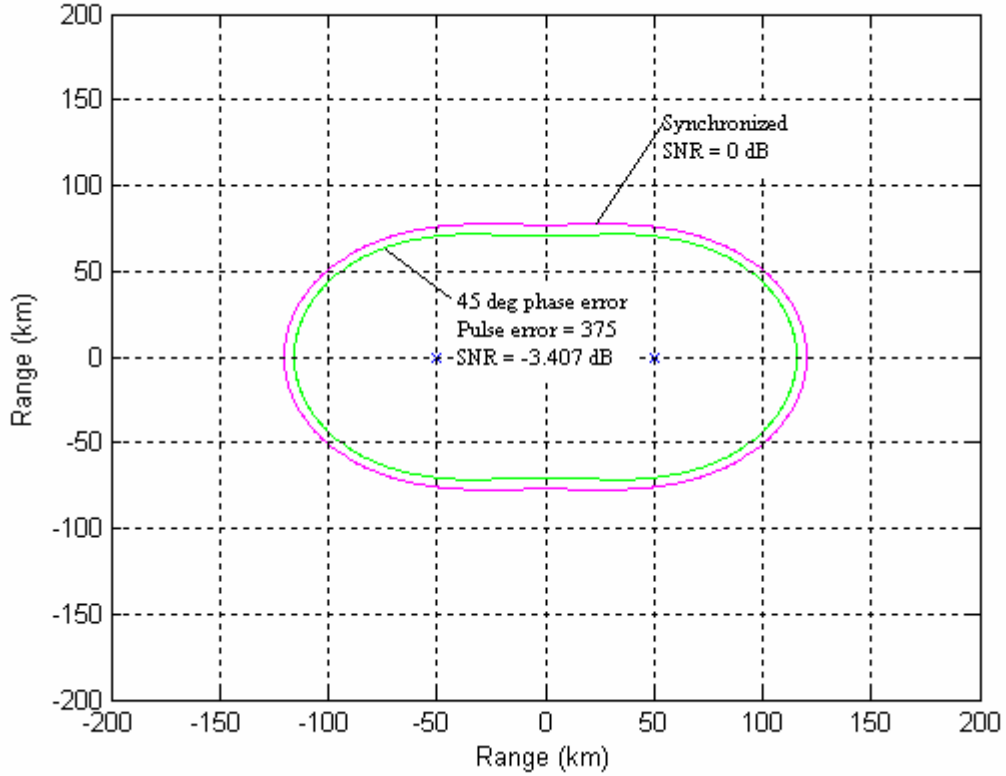
Figure 27.   Cassini curves plotted for a two-node distributed radar network with synchronized pulses (red) versus curves plotted for a 45° phase error and a pulse error of 375 time index values between the two combining pulses (green).

C.   SUMMARY AND DISCUSSION

This chapter has explored the issue of synchronization in a distributed radar network, focusing specifically on the requirements associated with synchronizing the reflected pulses. Phase and pulse synchronization have been explored, and their impact on received *SNR* has been presented graphically and numerically.

If pulses arrive perfectly synchronized at the target (complete overlap and in phase), then there is no destructive interference between them. If there is no overlap, the received pulse will have a signal power at least as great as the transmitted pulse; with complete overlap, the received pulse will have signal power twice that of the transmitted pulse. If the pulse overlap results in destructive interference, the received signal power will be less than that transmitted. Therefore, synchronization results in a range of possible received *SNR* gain values from 0 to n^2. Due to hardware constraints, these two extremes may not be achievable in practical applications.

V. CONCLUSION

This thesis explored the potential benefits of two, three, and four-node distributed radar networks with the potential to provide a received *SNR* proportional to n^2 times that of a single-node system, where n is the number of nodes in the network. By plotting the Cassini curves for these distributed radar networks along with the Cassini curves of a monostatic radar system for the same level of received *SNR*, these benefits were graphically demonstrated. The *SNR* gains resulted in a larger area of coverage for the distributed radar network compared to that of a power-equivalent monostatic radar. The impact of phase and pulse synchronization on a distributed radar network was also explored. By examining phase error and pulse error separately, and then examining their impact on the coverage areas of a two-node distributed radar network, the importance of synchronization to a distributed radar network was demonstrated.

A. CONTRIBUTIONS OF THIS THESIS

This thesis accomplished two objectives. The equations developed in [4] for plotting the Cassini ovals of a bistatic radar were extended to radar systems with $n = 3$ and $n = 4$. The Cassini curves were plotted for two, three, and four-node distributed radar networks and compared to those of a monostatic radar system for the same value of received *SNR*. The requirements associated with synchronization of a distributed radar network were examined and their impact on performance was presented.

This thesis expands the ideas in [4] beyond a traditional bistatic radar system to a system with $n = 3$ and $n = 4$. In doing so, specific equations for plotting the Cassini curves for a system with $n = 3$ and $n = 4$ are presented. Using these equations, a general equation is derived to plot Cassini curves for n nodes. The plots of Cassini curves for two, three, and four-node distributed radar networks are used to compare the performance of a distributed radar network to that of a monostatic radar. The performance gains of a distributed radar network are clearly demonstrated by observation of these plots. The assumption of synchronization across all transmitters and receivers is explored and the

51

requirements of phase and pulse synchronization are considered. The impact of phase and pulse synchronization on the coverage areas of a distributed radar network was illustrated, and the requirement to synchronize the network was demonstrated.

B.   RECOMMENDATIONS FOR FUTURE WORK

The research and simulations conducted in the thesis uncovered several areas for further work. The development of equations to plot the Cassini curves for $n = 3$ and $n = 4$ was based on *observation* of the derivation provided in [4] for the bistatic case. While a result based on observation was sufficient for the purposes of this thesis, a result that is supportable by complete derivation is preferable. An exploration into the equation to plot Cassini curves for n nodes that includes a complete derivation is recommended for further study.

The comparison of the coverage area of a distributed radar network with that of a monostatic radar was done through observation of the plotted Cassini curves for both systems. A numerical evaluation of the area within the Cassini curves is another means of comparing these systems. The derivation of equations to evaluate the area within Cassini ovals for a bistatic radar system is given in [4], and an extension of this work beyond the bistatic case to higher orders of systems is recommended for further study.

Finally, the investigation of synchronization presented here did not address Doppler and its effect on frequency synchronization, the effects of target cross section, or the effects of electromagnetic propagation in the medium between the distributed radar network and the target on the received *SNR*. This thesis assumes the distributed radar network operates with coherent integration and that there is zero target fluctuation loss [16]. In other words, the results presented here were fairly idealized. A study into one or more of these factors is suggested to further explore the potential of a distributed radar network.

APPENDIX

A. MATLAB CODE FOR MONOSTATIC.M

This appendix details the monostatic.m code developed to plot a monostatic Cassini curve in Figure 9 and evaluate the area of coverage for this system using Equation (2.3).

```
n=1;                                        %# of nodes
Pt=10^(10/10)/n;                            %dbW
Gt=10^(8/10);                               %dB
Gr=Gt;                                      %dB
c=3*10^8;                                    %m/s
f=10*10^9;                                   %Hz
lambda=c/f;                                  %m
sigma=10^(10/10);                           %dbsm
k=1.38065*10^(-23);                         %J/Kelvin
Ts=300;                                     %Kelvin
Ft=10^(-3.5/10);                            %dB
Fr=10^(-3.5/10);                            %dB
losses=1;                                   %dB
B=60*10^6;                                   %Hz
Noise=k*Ts*B*losses;
K=(Pt*Gt*Gr*lambda^2*sigma*Ft^2*Fr^2)/(Noise*(4*pi)^3);

x=[-150:150];                               %grid of
y=[-150:150];                               %ranges
[X,Y]=meshgrid(x,y);

R=sqrt(X.^2+Y.^2);
SNRdB=10*log10(K./R.^4);
V=[10^(6/10) 10^(9/10) 10^(12/10)];
figure(1)
c=contour(x,y,SNRdB,V,'b'); grid;hold
plot([0 0], [0 0], 'x');
axis equal;
axis([-150 150 -150 150])
hold on;
xlabel('Range (km)'); ylabel('Range (km)');

%Find area within each SNR contour
for SNR6=3.981
   R6=(K/(SNR6))^(1/4);
```

```
   i=find(R6<1.0);
   R(i)=1*ones(size(i));
   Area6=pi*(R6^2);
end
for SNR9=7.943
   R9=(K/(SNR9))^(1/4);
   i=find(R9<1.0);
   R(i)=1*ones(size(i));
   Area9=pi*(R9^2);
end
for SNR12=15.849
   R12=(K/(SNR12))^(1/4);
   i=find(R12<1.0);
   R(i)=1*ones(size(i));
   Area12=pi*(R12^2);
end

SNR1=[10^(6/10) 10^(9/10) 10^(12/10)]
area1=[Area6 Area9 Area12]
```

B.   MATLAB CODE FOR BISTATIC.M

This appendix details the bistatic.m code developed to generate and plot Cassini ovals for 2 nodes using Equation (2.14) and evaluate the area within the curves using Equation (2.6).

```
n=2;
theta=linspace(0,2*pi,10000);
d=100;                              %d=dist(km) btwn sensors
R=d/2;                              %R=dist(km) from a sensor to origin
Pt=10^(8.01/10);                    %dbW
Gt=10^(8/10);                       %dB
Gr=Gt;                              %dB
c=3*10^8;                           %km/s
f=10*10^9;                          %Hz
lambda=c/f;                         %km
sigma=10^(10/10);                   %dbsm
k=1.38065*10^(-23);                 %J/Kelvin
Ts=300;                             %Kelvin
Ft=10^(-3.5/10);                    %dB
Fr=10^(-3.5/10);                    %dB
losses=1;                           %dB
B=60*10^6;                          %Hz
Noise=k*Ts*B*losses;
```

```
K=(Pt*Gt*Gr*lambda^2*sigma*Ft^2*Fr^2)/( Noise*(4*pi)^3);

snr0 = 10*log10(16*K/(d^4));                    %lemniscate oval
snrm9 = snr0-9;                                 %outer cosite oval
snrm6 = snr0-6;                                 %middle cosite oval
snrm3 = snr0-3;                                 %inner cosite oval

snr2=[snr0 snrm3 snrm6 snrm9]

for isnr2=1:length(snr2)
  SNR=10^(snr2(isnr2)/10);                       %converts each value in snr
                                                 %from dB to ratio, for operations

  SNR0=10^(snr0/10);
  SNRm9=10^(snrm9/10);
  SNRm6=10^(snrm6/10);
  SNRm3=10^(snrm3/10);

  %RtRr (bistatic max range constant)
  RtRr0=sqrt(K/SNR0);                            %lemniscate oval
  RtRrm9=sqrt(K/SNRm9);                          %outer cosite oval
  RtRrm6=sqrt(K/SNRm6);                          %middle cosite oval
  RtRrm3=sqrt(K/SNRm3);                          %inner cosite oval
 end

  i=i+1; k=0;
% calculate a for each contour
  a0=((sqrt(RtRr0))/R).^(4); am9=((sqrt(RtRrm9))/R).^(4);
  am6=((sqrt(RtRrm6))/R).^(4); am3=((sqrt(RtRrm3))/R).^(4);

%Plot each case
  R0=(cos(n.*theta)+sqrt(a0+cos(n.*theta).^2-1));     %lemniscate
  r0=(R)*((R0).^(1/n));
  X=r0.*cos(theta);
  Y=r0.*sin(theta);
  figure(2)
  plot(X,Y)
  hold on

  Rm9=(cos(n.*theta)+sqrt(am9+cos(n.*theta).^2-1));   %outer cosite
  rm9=(R)*((Rm9).^(1/n));
  X=rm9.*cos(theta);
  Y=rm9.*sin(theta);
  plot(X,Y)

  Rm6=(cos(n.*theta)+sqrt(am6+cos(n.*theta).^2-1));   %middle cosite
  rm6=(R)*((Rm6).^(1/n));
```

```
X=rm6.*cos(theta);
Y=rm6.*sin(theta);
plot(X,Y)

Rm3=(cos(n.*theta)+sqrt(am3+cos(n.*theta).^2-1));   %inner cosite
rm3=(R)*((Rm3).^(1/n));
X=rm3.*cos(theta);
Y=rm3.*sin(theta);
plot(X,Y)
```

```
grid
xlabel('Range (km)'), ylabel('Range (km)')
axis([-100 100 -100 100])
axis equal
```

```
%Find area within each SNR contour
Area0=2*RtRr0;
Aream3=pi*RtRrm3*(1-(1/64)*((d^4)/(RtRrm3^2))-(3/16384)*((d^8)/(RtRrm3^4)));
Aream6=pi*RtRrm6*(1-(1/64)*((d^4)/(RtRrm6^2))-(3/16384)*((d^8)/(RtRrm6^4)));
Aream9=pi*RtRrm9*(1-(1/64)*((d^4)/(RtRrm9^2))-(3/16384)*((d^8)/(RtRrm9^4)));
```

```
Area=[Area0  Aream3  Aream6  Aream9]
```

C.   MATLAB CODE FOR NETTEDCONTOURS_2NODES.M

This appendix details the nettedcontours_2nodes.m code developed to generate and plot Cassini ovals for 2 nodes with monostatic operation, bistatic operation, and netted operation using Equation (2.7). The bistatic case (Figure 10) is plotted and its area evaluated. By changing the value of *n*, the Cassini ovals for 3 and 4 nodes can be plotted as well.

```
n=2                                     %# nodes
Pt=10^(10/10)/n;                        %dbW
Pt=10^(10/10);                          %Figure 10 bistatic case
Gt=10^(8/10);                           %dB
Gr=Gt;                                  %dB
c=3*10^8;                               %m/s
f=10*10^9;                              %Hz
lambda=c/f;                             %m
sigma=10^(10/10);                       %dbsm
k=1.38065*10^(-23);                     %J/Kelvin
Ts=300;                                 %Kelvin
Ft=10^(-3.5/10);                        %dB
```

```
Fr=10^(-3.5/10);                                      %dB
losses=1;                                             %dB
B=60*10^6;                                            %Hz
Noise=k*Ts*B*losses;
SN=1;
K=(Pt*Gt*Gr*lambda^2*sigma*Ft^2*Fr^2)/(SN*Noise*(4*pi)^3);

x1=[-200:200];
y1=[-200:200];
[X1,Y1]=meshgrid(x1,y1);

R1=sqrt((X1+50).^2+Y1.^2);
SNRM1=(K./R1.^4);

R2=sqrt((X1-50).^2+Y1.^2);
SNRM2=(K./R2.^4);

SNRMT=SNRM1+SNRM2;

% Bistatic
SNRB=K./((R2.^2).*(R1.^2));
SNRBT = 2*SNRB;

SNRT = SNRBT + SNRMT;

V=[10^(6/10) 10^(9/10) 10^(12/10)];                   %SNRdB=6,9,12
V1=[10^(6/10)];V2=[10^(9/10)];V3=[10^(12/10)];

%Monostatic operation
figure(1)
c2=contour(x1,y1,SNRMT,V,'b');hold
plot([-50 50], [0 0], 'x')
axis equal;
axis([-150 150 -150 150])
xlabel('Range (km)'); ylabel('Range (km)');
grid

%Bistatic operation
figure(2)
% c3=contour(x1,y1,SNRBT,V,'b');hold              %plots total bistatic w/2Txs
c3=contour(x1,y1,SNRB,V,'b');hold                 %plots bistatic w/1Tx (Fig 10)
plot([-50 50], [0 0], 'x')
axis equal;
axis([-150 150 -150 150])
xlabel('Range (km)'); ylabel('Range (km)');
grid; hold
```

R1R2=sqrt(K./15.849)
AreaB12=pi*R1R2*(1-(1/64)*((d^4)/(R1R2^2))-(3/16384)*((d^8)/(R1R2^4)))   %Fig10

%Netted operation
figure(3)
c3=contour(x1,y1,SNRT,V,'b');
axis([-150 150 -150 150])
xlabel('Range (km)'); ylabel('Range (km)');
grid; hold

%Node plots
plot([-50 50], [0 0], 'x')

%Monostatic - (0,0)
Xr1=0; Yr1=0;
R1=sqrt((X1-Xr1).^2+(Y1-Yr1).^2);
SNRM=(n*K./R1.^4);
c3=contour(x1,y1,SNRM,V,'r');
plot([0 0], [0 0], 'xr')
axis equal
axis([-150 150 -150 150])
hold

LIST OF REFERENCES

1. Jayasimha, D.N, Iyengar, S.S., and Kashyap, R.L, "Information Integration and Synchronization in Distributed Sensor Networks," IEEE Transactions on Systems, Man, and Cybernetics, Vol 21, No 5, 1991.

2. Baker, C. J. and Hume, A. L., "Netted Radar Sensing," *Proceedings of the CIE International Radar Conference*, pp. 110-114, 2001.

3. Akyldiz, I.F., Su, W., Sankarasubramaniam, Y., and Cayirci, E., "A Survey on Sensor Networks," IEEE Communications Magazine, 2002.

4. Willis, N.J., *Bistatic Radar*, Technology Service Corporation, Maryland, 1995.

5. Radar. (2006). In *Wikipedia, The Free Encyclopedia*. Retrieved June 7, 2006 from http://en.wikipedia.org/w/index.php?title=Radar&oldid=57244529

6. Wassenaar, J. (2003). In *Cassini Curve*. Retrieved June 7, 2006 from http://www.2dcurves.com/higher/highercc.html

7. Weisstein, E.W. (1999). In *Equilateral Triangle*. Retrieved June 7, 2006 from http://mathworld.wolfram.com/EquilateralTriangle.html

8. Weisstein, E.W. (1999). In *Square*. Retrieved June 7, 2006 from http://mathworld.wolfram.com/Square.html

9. Knorr, J.B., private conversation at the Naval Postgraduate School, June 12, 2006.

10. Therrien, C.W., and Tummala, M., *Probability for Electrical and Computer Engineers*, CRC Press, New York, 2004.

11. Akyldiz, I.F, and Su, W., "Time-Diffusion Synchronization Protocol for Wireless Sensor Networks," IEEE/ACM Transactions on Networking, Vol 13, No 2, 2005.

12. Li, Q., and Rus, D., "Global Clock Synchronization in Sensor Networks," IEEE Transactions on Computers, Vol 55, No 2, 2006.

13. Chernyak, V.S., *Fundamentals of Multisite Radar Systems: Mulistatic Radars and Multiradar Systems*, Gordon and Breach Science Publishers, Canada, 1993.

14. Walker, T.O., Tummala, M., and Michael, J.B., "Pulse Transmission Scheduling for a Distributed System of Cooperative Radars," *Proceedings of the IEEE International Conference on Systems of Systems Engineering*, Los Angeles, CA, April 2006.

15.   Halliday, D., Resnick, R., and Walker, J., *Fundamentals of Physics*, John Wiley and Sons, New York, 1997.

16.   Skolnik, M.L., *Introduction to Radar Systems*, McGraw Hill, Boston, 2001.

INITIAL DISTRIBUTION LIST

1. Defense Technical Information Center
   Ft. Belvoir, Virginia

2. Dudley Knox Library
   Naval Postgraduate School
   Monterey, California

3. Marine Corps Representative
   Naval Postgraduate School
   Monterey, California

4. Director, Training and Education, MCCDC, Code C46
   Quantico, Virginia

5. Director, Marine Corps Research Center, MCCDC, Code C40RC
   Quantico, Virginia

6. Marine Corps Tactical Systems Support Activity (Attn: Operations Officer)
   Camp Pendleton, California